FORWARD PROBLEM OF ELECTROCARDIOGRAPHY IN TERMS OF 3D TRANSMEMBRANE POTENTIALS USING COMSOL

A THESIS SUBMITTED TO
THE GRADUATE SCHOOL OF NATURAL AND APPLIED SCIENCES
OF
MIDDLE EAST TECHNICAL UNIVERSITY

BY

GIZEM BEDIR

IN PARTIAL FULFILLMENT OF THE REQUIREMENTS
FOR
THE DEGREE OF MASTER OF SCIENCE
IN
BIOMEDICAL ENGINEERING

JANUARY 2015

Approval of the thesis:

FORWARD PROBLEM OF ELECTROCARDIOGRAPHY IN TERMS OF 3D TRANSMEMBRANE POTENTIALS USING COMSOL

submitted by **GIZEM BEDIR** in partial fulfillment of the requirements for the degree of **Master of Science in Biomedical Engineering Department, Middle East Technical University** by,

Prof. Dr. Gülbin Dural Ünver
Dean, Graduate School of **Natural and Applied Sciences** _____

Prof. Dr. Hakan Işık Tarman
Head of Department, **Biomedical Engineering** _____

Assoc. Prof. Dr. Yeşim Serinağaoğlu Doğrusöz
Supervisor, **Electrical and Electronics Eng. Dept., METU** _____

Assist. Prof. Dr. Barbaros Çetin
Co-supervisor, **Mechanical Eng. Dept., Bilkent Uni.** _____

Examining Committee Members:

Prof. Dr. Nevzat Gençer
Electrical and Electronics Engineering Department, METU _____

Assoc. Prof. Dr. Yeşim Serinağaoğlu Doğrusöz
Electrical and Electronics Engineering Department, METU _____

Assoc. Prof. Dr. Lale Alatan
Electrical and Electronics Engineering Department, METU _____

Assist. Prof. Dr. Barbaros Çetin
Mechanical Engineering Department, Bilkent Uni. _____

Assist. Prof. Dr. Özlem Birgül
Biomedical Engineering Department, Ankara Uni. _____

Date: _____

I hereby declare that all information in this document has been obtained and presented in accordance with academic rules and ethical conduct. I also declare that, as required by these rules and conduct, I have fully cited and referenced all material and results that are not original to this work.

Name, Last Name: GIZEM BEDIR

Signature :

ABSTRACT

FORWARD PROBLEM OF ELECTROCARDIOGRAPHY IN TERMS OF 3D TRANSMEMBRANE POTENTIALS USING COMSOL

Bedir, Gizem

M.S., Department of Biomedical Engineering

Supervisor : Assoc. Prof. Dr. Yeşim Serinağaoğlu Doğrusöz

Co-Supervisor : Assist. Prof. Dr. Barbaros Çetin

January 2015, 54 pages

Computation of body surface potentials from equivalent cardiac sources is called as forward problem of electrocardiography (ECG). There exist different solution methods for solving the forward ECG problem. These solution methods depend on the choice of the equivalent cardiac sources. In this study, bidomain model based transmembrane potential (TMP) distribution is used as equivalent cardiac source to examine the cellular electrophysiology macroscopically. With this type of source definition, the TMP values are linearly related to the body surface potentials, and this linear relationship is modeled by a forward transfer matrix, T. Then the forward problem of ECG is solved in order to obtain T, using finite element method (FEM).

In the first part of this study, both the heart and torso are assumed as two concentric spheres and electrically isotropic regions. First forward problem of ECG is solved both analytically and numerically, and then a transfer matrix that relates the TMPs to the body surface potentials is constructed. Accuracy of the transfer matrix is verified by the analytical solution. Numerical solutions are done using COMSOL Multiphysics Software which provides easy mesh generation by discretizing the solution domain with FEM. Flexibility of arranging both mesh element sizes and numbers in the solution domain makes COMSOL preferable for this study. In the second part of the study, a spherical heart is placed inside a realistic torso geometry and the forward problem is solved again to obtain the transfer matrix.

Keywords: Electrocardiogram, Forward Problem, Transfer Matrix, Finite Element Method, Numerical Simulation, COMSOL, Analytical Solution

ÖZ

3 BOYUTLU TRANSMEMBRAN POTANSİYELLERİ CİNSİNDEN COMSOL KULLANARAK ELEKTROKARDİYOGRAFİDE İLERİ PROBLEM

Bedir, Gizem
Yüksek Lisans, Biyomedikal Mühendisliği Bölümü
Tez Yöneticisi : Doç. Dr. Yeşim Serinağaoğlu Doğrusöz
Ortak Tez Yöneticisi : Yrd. Doç. Dr. Barbaros Çetin

Ocak 2015 , 54 sayfa

Kalpteki eşdeğer elektriksel kaynaklardan gövde yüzeyindeki potansiyellerin hesaplanması elektrokardiyografide (EKG) ileri problem olarak adlandırılır. EKG ileri problemini çözmek için birçok farklı çözüm yöntemi vardır. Bu çözüm yöntemleri seçilen eşdeğer kalp kaynaklarına göre değişir. Bu çalışmada hücresel elektrofizyolojiyi makroskopik olarak inceleyebilmek için bidomain modele dayanan transmembran potansiyel dağılımı eşdeğer kaynak olarak kullanılmıştır. Bu kaynak tanımıyla, transmembran potansiyel değerleri kalp yüzeyindeki potansiyellerle doğrusal olarak ilişkilendirilmiştir ve bu ilişkilendirme ileri problem transfer matrisi T ile modellenmiştir. Daha sonra, T matrisini elde edebilmek için kalpte ileri problem çözülmüştür. Bu problemi çözmek için sonlu elemanlar metodu kullanılmıştır.

Bu çalışmanın ilk kısmında hem kalp hem de gövde iki adet eş merkezli ve elektriksel olarak eş yönlü küresel bölgelerle temsil edilmektedir. İlk olarak, kalpte ileri problem analitik ve sayısal olarak çözülmüştür, daha sonra transmembran potansiyellerini vücut yüzeyi potansiyelleriyle ilişkilendiren T matrisi oluşturulmuştur. Bu matrisin doğruluğu analitik çözümlerle kanıtlanmıştır. Sayısal çözümler sonlu elemanlar yöntemini kullanarak çözüm alanını sonlu elemanlara bölen COMSOL Multiphysics Software programıyla yapılmıştır. COMSOL programı sonlu elemanların boyutunu ve sayısını ayarlamada sağladığı kolaylıktan dolayı tercih edilmiştir. Çalışmanın ikinci aşamasında ise küre ile temsil edilen kalp gerçekçi gövde geometrisinin

içine yerleştirilmiş ve ileri problem çözümüyle tekrar T matrisi elde edilmiştir.

Anahtar Kelimeler: Elektrokardiyogram, İleri Problem, Transfer Matris, Sonlu Elemanlar Metodu, COMSOL, Analitik Çözüm

To my grandparents

Birsen Bölek and Mustafa Bölek

ACKNOWLEDGMENTS

First of all, I would like to thank my supervisor Assoc. Prof. Yeşim Serinağaoğlu Doğrusöz for her constant support, guidance and friendship. It was a great honor to work with her for the last two years and our cooperation influenced my academical and world view highly. I also would like to thank Assist. Prof. Barbaros Çetin for his support and guidance. He not only supported me on my research but also motivated and influenced me highly in scientific context. His ideas and support made it possible that in a short time I were able to build the frame of this work.

I also would like to thank Kadir Gökhan Güler for his support and valuable feedback for the future of this resarch, which I very appreciate.

Finally, I would like to thank specially my mother Sevda Bölek for her endless love and my aunt Gamze Tuna for making me happy by giving her positive thoughts and energy to me at my stressful times.

This study is part of the project 111E258 that is supported by Turkish Scientific and Technological Research Council (TUBITAK).

TABLE OF CONTENTS

LIST OF TABLES

TABLES

LIST OF FIGURES

FIGURES

CHAPTER 1

INTRODUCTION

In today's world, heart diseases are one of the most widespread causes of mortality. According to World Health Organization (WHO) reports, each year approximately 17 million people die due to cardiovascular diseases all over the world [2]. Therefore, understanding the functioning of the heart becomes more important issue for scientists to be able to develop effective diagnostic tools and therapies for people suffering from heart diseases.

Electrocardiogram (ECG) is the recording of the heart's electrical activity from the body surface as electric potential [3]. Each change in the electrical activity within the heart reflects a variation on the resultant ECG. That is why ECG is a major tool to interpret the functioning of the heart and diagnose the heart diseases.

The relation between the heart's electrical activity and the resultant ECG can be studied under two major problems; these are the forward and inverse problems of ECG. Obtaining electrical potentials from the equivalent heart sources is called as the forward problem of ECG and reconstruction of the equivalent cardiac sources by using the measured ECG from the body surface is called as the inverse problem of ECG. Inverse problem is very important to understand the electrical activity of the cardiac tissue. It enables noninvasive diagnosis for the heart diseases by providing distribution of cardiac sources within the heart only using measurements from the body surface.

According to the selected equivalent cardiac sources, the problem can be either linear or nonlinear. In this study, transmembrane potential (TMP) distribution is selected

as equivalent cardiac source and the problem becomes linear. By using this linearity, forward transfer matrix which contains information about the electrical conductivity and geometry of a volume conductor that is specific to each patient is obtained and inverse problem is solved [4].

As long as there is no change at electrical conductivity and geometry of a volume conductor, there is no need to construct transfer matrix again and again. Because, the forward transfer matrix carries only static information about volume conductor of each patient. Therefore, if the volume conductor is same, it is unnecessary to construct a new transfer matrix for different TMP distributions within the heart.

1.1 Scope of the Thesis

Depending on the equivalent cardiac sources, there exist different solution methods for the ECG forward problem. In this study, bidomain model based transmembrane potential (TMP) distribution is used as equivalent cardiac source in order to examine the cellular electrophysiology macroscopically. With this type of source definition, the TMP values are linearly related to the body surface potentials, and this linear relationship is modeled by a forward transfer matrix, T as indicated in the previous section. Then the forward problem of ECG is solved to construct T. In the first part of the study, both the heart and torso are assumed as two concentric spheres and electrically isotropic regions. First, the forward problem of ECG is solved analytically and numerically. For numerical solutions, finite element method (FEM) is used. Secondly, TMP based transfer matrix, T is constructed by using point cloud modeling. Then the accuracy of T is verified by direct forward solutions. In the second part of the study, a spherical heart is placed inside of a realistic torso to show the applicability of the point cloud modeling to any irregular geometry. By this purpose, the forward problem is solved and T is constructed again.

In this study, numerical solutions are carried out in COMSOL Multiphysics Software, which provides easy mesh generation by discretizing the solution domain using FEM. Flexibility of arranging both mesh element sizes and numbers in the solution domain makes COMSOL preferable for this study.

1.2 Contribution of the Thesis

In this thesis, T matrix which directly relates TMPs within the heart to the body surface potentials is constructed by point cloud modeling. Although the idea of point cloud modeling comes from another study [5], this thesis makes contribution to the literature by verifying the results of the point cloud modeling with analytical solution that is also derived by us. Although COMSOL is used for mesh generation, MATLAB code for point cloud modeling is written to construct T by using MATLAB Livelink of COMSOL. In addition to these, the results of analytical solution and point cloud modeling are analyzed according to mesh sensitivity and the density of the nodes in the point cloud modelling respectively.

1.3 Outline of the Thesis

Second chapter gives background information about the anatomy and electrophysiology of the heart and discusses related studies in the literature. Finally, formulation of the forward problem is introduced.

Third chapter starts with theoritical explanation of the forward problem and continues with related analytical and numerically done point cloud modeling solutions by discussing their results.

Fourth chapter shows applicability of point cloud modeling to any irregular geometry by using realistic torso with spherical heart.

Chapter five summarizes the study done in the thesis and discusses future work.

CHAPTER 2

BACKGROUND INFORMATION

This chapter gives background information about the anatomy and electrophysiology of the heart. Then the equivalent cardiac sources and numerical solution methods for the forward problem of electrocardiography (ECG) are discussed. Finally, formulation of the forward problem is introduced.

2.1 Anatomy of the Heart

The heart is one of the most important organs and the most powerful muscle in the human body. It behaves like a strong electromechanical pump, which has contraction feature by its own accord. The main duty of this pump is to provide oxygen and nutrition rich blood throughout the entire body. Removing metabolic wastes, regulating body temperature and protecting acid-base balance of the body are some of other important functions of the heart [6].

Heart is found at the center of the chest and is composed of three layers of muscle tissue. Heart muscles are called as endocardium, myocardium and epicardium from inside to outside (Figure 2.1) [7]. In humans and other mammals, cardiac muscle is divided into four chambers: the upper part of the cardiac muscle contains right and left atria and the lower part contains right and left ventricles. Heart chambers have some vital roles during heart contraction. In addition to the chambers of the heart, there are also valves between the chambers, which allow blood flow in or out [8].

In general, upper chambers receive incoming blood; right atrium receives oxygen

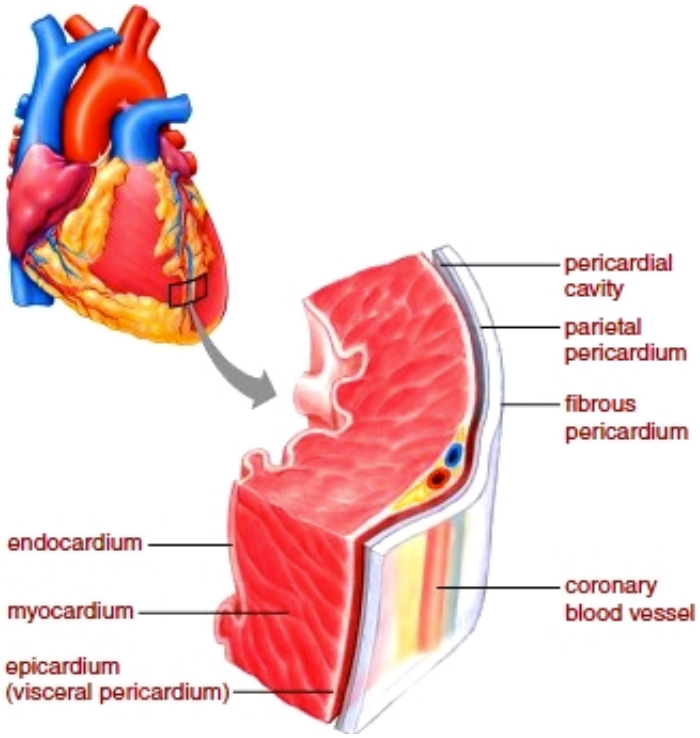

Figure 2.1: Cardiac Muscle [9]

poor blood from the superior and inferior vena cava, which are large diameter veins. These veins carry this de-oxygenated blood from the upper and lower parts of the body respectively. After receiving de-oxygenated blood, right atrium pumps it to the right ventricle. Left atrium, on the other hand, receives oxygen rich blood from the lungs by pulmonary veins and then pumps it to the left ventricle. In contrast to the upper chambers, lower chambers pump blood out of the heart; right ventricle pumps oxygen poor blood to the lungs by pulmonary artery and left ventricle pumps oxygen rich blood throughout the body by aorta [6]. The four chambers of the heart and the main arteries which carry blood can be seen better from Figure 2.2.

2.2 Electrical Activity of the Heart

This section gives brief background information about the electrical activity of the heart starting from cellular electrophysiological level and continuing with the electrocardiography.

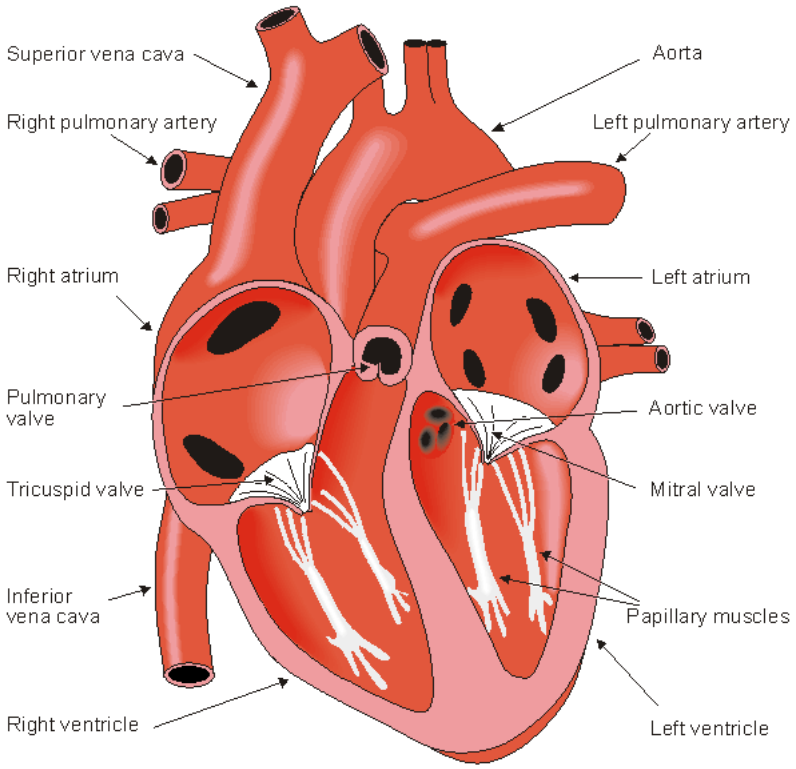

Figure 2.2: Anatomy of the Heart [3]

2.2.1 Action Potential Generation

There are two types of cells in the cardiac muscle: the cardiac pacemaker cells and cardiomyocytes [7]. Electrical activation within the heart is initiated by cardiac pacemaker cells. These cells are responsible for generation and transmission of electrical impulses. The cardiomyocytes, on the other hand, are the cells that form cardiac muscle and they provide the necessary contraction for the heart beat after electrical stimulation by cardiac pacemaker cells. Electrical activation in cardiac cells is generated as a result of the ionic movements across the cell membrane. This movement causes a potential difference between the intracellular and the extracellular space called as transmembrane potential [10]:

$$\phi_m = \phi_i - \phi_e \tag{2.1}$$

At resting state, these cells have a transmembrane potential around -80 mV. The in-

flow of sodium ions from cell membrane causes depolarization of these cells and the resting potential immediately changes from -80 to +20 mV and action potential is generated. Cardiac depolarization is followed by a plateau phase due to the inflow of calcium and outflow of potassium ions. This phase determines the duration of the action potential and this duration shows variance at different regions of the cardiac tissue. As a consequence of the outflow of potassium ions, plateau phase is followed by repolarization phase and TMP of the cell changes back to its resting potential, -80 mV [10]. Figure 2.3 shows typical action potential waveform of ventricular cardiomyocyte.

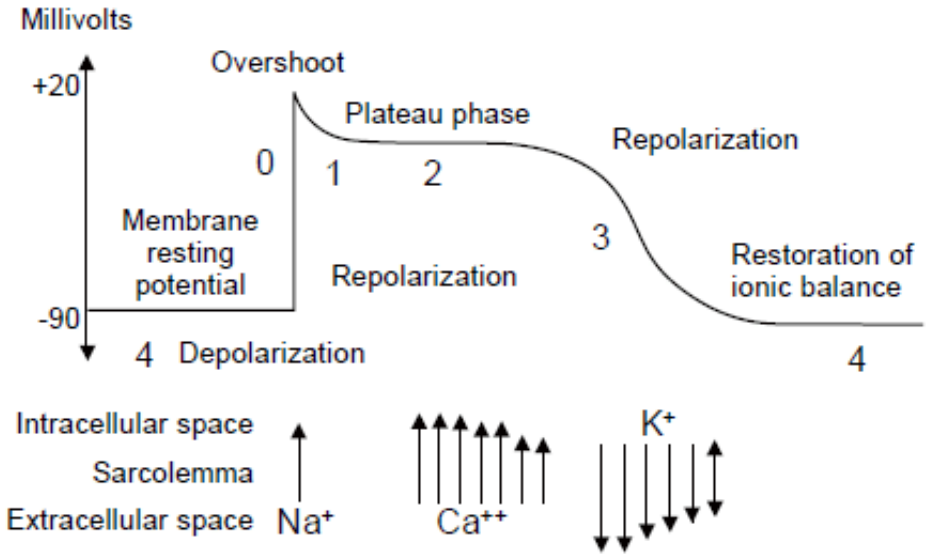

Figure 2.3: Action Potential of Standard Cardiomyocyte [11]

2.2.2 Conduction System of the Heart

Heart has a natural pacemaker called as sino-atrial (SA) node or sinus node where the impulse generation starts initially [3]. This pacemaker is composed of a group of specialized cells called as cardiac pacemaker cells that are briefly explained in the previous section. This specialized group of cells are located at the upper part of the right atrium.

After the impulse generation in the SA node, electrical conduction propagates throughout the other parts of the cardiac muscle by following a special conduction path. The

action potential is firstly spread to the right atrium and the left atrium by Bahmann's bundle. Since there is no direct electrical connection between the atria and the ventricles, the action potential propagates from the atria to the ventricles by atrio-ventricular (AV) node. Then, the activation in the AV node is transmitted to the ventricles by specialized conduction system namely bundle of His and Purkinje fibers [3].

Each region in cardiac muscle has different excitatory feature. That means the action potential generated throughout the conduction pathway between the SA node and the ventricles shows different waveform characteristic. Since action potential generation first starts in the SA node and then propagates to the ventricles, there must be a delay between the excitation times of each region. Fig. 2.4 shows this varying action potential waveform at different regions of the heart.

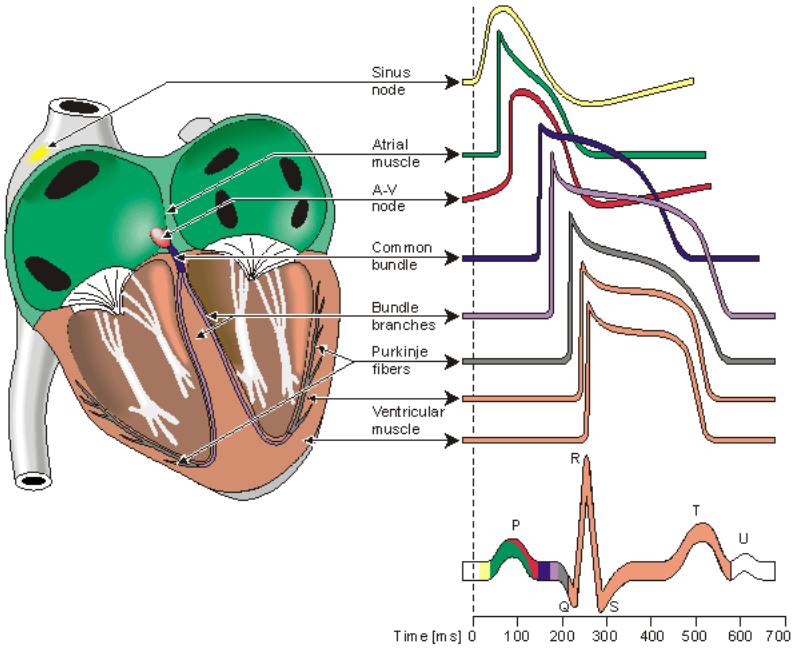

Figure 2.4: Electrical Conduction System of the Heart [3]

2.2.3 Electrocardiography

Noninvasive recording of the heart's electrical activity from the body surface is called as electrocardiography (ECG or EKG) and the resultant record is defined as electrocardiogram. The additive sum of the all action potentials generated at different re-

gions of the cardiac tissue forms the electrocardiogram (Figure 2.4). During normal record, there occur P, Q, R, S, and T waves in ECG [3].

P wave is generated as a result of the atrial depolarization. After atrial depolarization, excitation wave front moves to the ventricles and leaves the atria that causes atria to repolarize. The repolarization of atria and depolarization of ventricles form QRS complex of the ECG. Finally, repolarization of ventricles constitutes T wave. Any abnormalities in the electrical activity of the heart affect the waveform of the resultant ECG.

The term ECG was first introduced by Willem Einthoven in 1903 and with this invention he received the Nobel Prize in Medicine [12]. Nowadays, the most widely used ECG is 12-lead ECG. 12 lead ECG shown in Figure 2.5 is composed of two groups of leads which are limb leads and precordial leads. Limb leads are composed of standard limb leads and augmented limb leads. The standard limb leads I, II and III are generated from the electrodes located on the right arm (RA), left arm (LA) and the left leg (LL). The augmented limb leads a_{VR}, a_{VL} and a_{VF} are also derived from the same electrode locations where the standard limb leads are generated from [13]. However, in contrast to the standard limb leads, the augmented limb leads provide the view of the heart's electrical activity from different angles but with a very small signal. Therefore, the signals coming from these leads are augmented as the name implies. Precordial leads from V_1 to V_6 are horizontally located on the chest. Since they are close enough to the heart, there is no need for augmentation. All signals coming from each of these 12 leads from a healthy subject are shown in Figure 2.6.

In addition to this standard 12 Lead ECG, some researchers use body surface potential mapping (BSPM). BSPM uses extended measurement points from both anterior and posterior parts of the body surface (Figure 2.7) [5]. Generally, the number of electrodes located on these measurement points is selected between 32 and 352. BSPM provides more detailed examination on heart's electrical activity. By using this mapping, the effects of small heart rhythm variations can also be detected easily from the body surface.

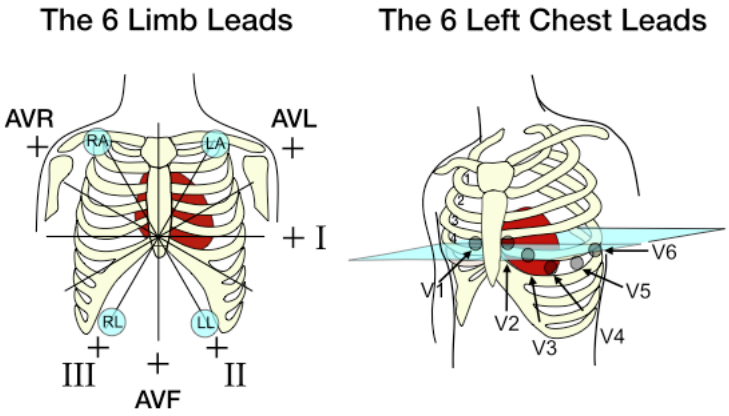

Figure 2.5: Limb Leads and Precordial Leads [14]

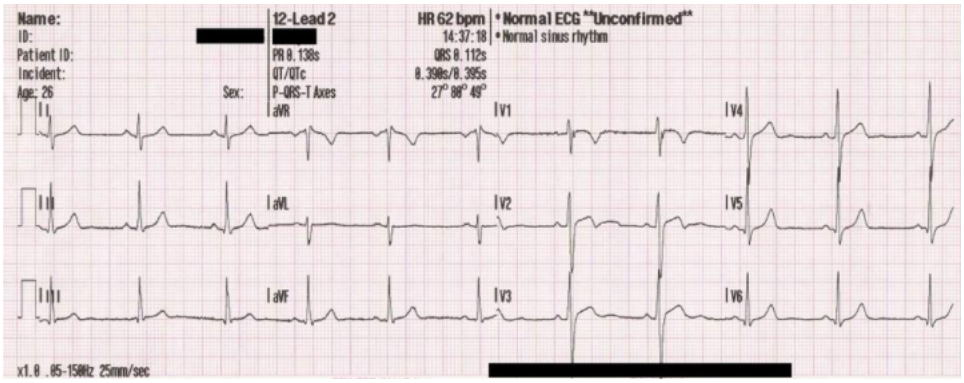

Figure 2.6: 12 Lead Electrocardiography from a Healthy Subject [15]

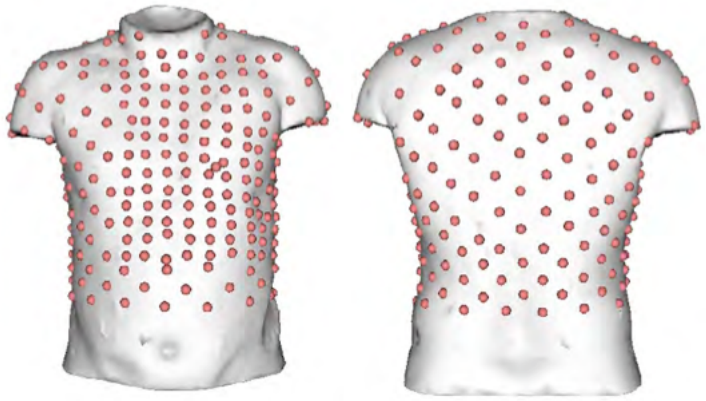

Figure 2.7: 352 sites of BSPM recording [5]

2.3 Problems of Electrocardiography

Computation of the body surface potentials from equivalent heart sources by using the theory of electromagnetism is called as the forward problem of electrocardiography (ECG) and the inverse problem of ECG restores the electrical activity within the heart from a given set of body surface potentials obtained by the forward problem [16]. The main application areas of the forward problem are **(i)** obtaining transfer matrix for the inverse problem, **(ii)** exploring the effects of electrophysiological properties (electrical conductivity, anisotropy, geometry etc) of the heart on the resultant ECG, and **(iii)** electrode location optimization for ECG recording [5].

Solution of the forward problem of ECG is composed of basically two main stages which are defining electrical activity of the heart in terms of equivalent sources and numerical solution of the problem.

2.3.1 Electrical Activity of the Heart in terms of Equivalent Sources

The electrical activity of the heart can be represented as either equivalent current dipoles or known potentials on the surface of the heart (epicardium, endocardium) or within the heart (transmembrane potentials). There are four types of equivalent dipole sources: fixed dipole, moving dipole, multiple dipole and multipole [17]. All of these equivalent cardiac sources have both advantages and disadvantages. In this study, TMP distributions are used as equivalent cardiac sources for their convenience with bidomain model (a heart tissue model) and for their significant advantages which will be given later.

Dipole source is composed of two equal in magnitude and opposite in sign point charges (monopoles) separated by a small distance. Since dipole is a vector, direction of a current dipole is from current sink to source. Fixed dipole source has a fixed location, but varying magnitude and orientation. There are three independent variables in a fixed dipole source due to the variation in magnitude thereby in orientation. Adding varying location feature to a fixed dipole makes it a moving dipole. Combination of several fixed dipoles at different locations of the heart is called as multiple dipoles. As described above, dipole source is formed by, two equal in magnitude and oppo-

site in sign monopoles. If dipole sources are used instead of monopoles, multipole is formed. Multipoles are very important, because any source can be represented by combining multipoles [3].

The electrical activity of the heart can be represented by using any of these equivalent dipole sources described above. Use of a fixed dipole source or a moving dipole source may not be enough to represent the electrical activity at each region of the heart. Therefore multiple dipole source or multipole source is used for better representation of this electrical activity and accuracy of the model increases. However, due to the complexity of these dipoles, there may occur some computational difficulties during problem solution.

In addition to point-like dipole sources, there are also distributed surface source models such as uniform double layer (UDL) model, equivalent double layer (EDL) model, epicardial and endocardial potential (EP) models [17]. Uniform double layer model is the representation of the ventricular depolarization. This model reflects activation wave front on ventricles by elementary current dipole sources that are oriented in the normal direction within the myocardium. Since it is really hard to obtain the electrical activity within the heart, it is more convenient to use a representative model for a surface, which encloses the myocardium. Therefore, equivalent double layer (EDL) model is introduced. This model exemplifies the electrical activity during ventricular depolarization on the epicardium and endocardium layer of the cardiac muscle and is equal to UDL model based on the solid angle theory. Although equivalent double layer model provides better representation than point like models, it gives no information about repolarization and recovery periods of the electrical activity of the heart [18]. Use of epicardial and endocardial potentials (EP) compensates this shortcoming of the EDL model by recovering the potential on the heart surface at any location during any instant of the cardiac cycle. EPs can also be measured from the heart surface invasively and this capability provides the verification of the inverse solutions. Another important advantages of using EPs are uniqueness of the solution and linearity of the problem. Neglecting blood masses within the myocardium is also another benefit of the EP model, because complexity of the problem decreases. However, EP model has some disadvantages such as problem becomes highly ill-posed due to the effects of smoothing and discretization on the surface potentials passing through the

torso [19]. Another disadvantage of the EP model is that it shows high sensitivity to errors on the introduced geometry [18].

As previously explained in section 2.2.1, TMPs are formed as a result of the potential differences between the intracellular and extracellular spaces within the myocardium due to generated moving action potentials. All other surface models: UDL, EDL and EP can be obtained from TMPs, since the TMP is the first potential distribution generated within the heart [17]. One of the most important advantages of using TMP distribution is that problem becomes linear and this linearity provides easiness for the solutions. Another benefit of TMP based formulation of the forward problem is the ability to obtain diseases in the heart by considering the distribution and shape of the TMPs as a result of the inverse problem solutions. Nevertheless, there are some limitations of the TMP based solutions such as the inverse solution is non-unique and therefore meaningless, but by using some additional constraints it is also possible to remove the non-uniqueness of the problem. Another disadvantage is the impossibility of measuring real TMPs within the myocardium, so the inverse problem solutions can not be verified. Therefore, some ionic current and flux models are introduced to represent the equivalent TMP distributions within the myocardium. These models can also be used for direct forward problem calculations. Since the first aim of this study is constructing transfer matrix for the inverse problem, these ionic current models, which mimic the real equivalent TMP distributions will not be discussed here.

2.4 Numerical Solution of the Forward Problem

Due to irregular geometry of heart and torso, analytical solution of the forward problem is not possible. Therefore, an appropriate numerical solution algorithm is needed. There are mainly two approaches for numerical solution of the problem, namely surface and volume methods [20].

Surface methods are capable of solving the regions, which have isotropic conductivities. In these methods, only the boundaries between different regions of the solution domain are being taken into consideration. Therefore, these methods are usually known as boundary element methods (BEM) [21, 22, 23]. If there are regions with

anisotropic conductivities in the solution domain, then forward calculations are done by getting an average isotropic conductivity of the regions. That means instead of anisotropic conductivities, their approximately equivalent average isotropic conductivities are used. Solution of the surface methods is based on integral equations [20], which are formulated form of linear partial differential equations. Volume methods, on the other hand, provide a solution for both isotropic and anisotropic regions. In volume methods, there is a three dimensional representation of the solution domain and all of the regions inside the torso are modeled entirely by contrast to BEM [24].

Surface methods seem to have less number of elements, since they only discretize the boundaries between different regions in a solution domain. However, surface methods combine the potential at each element to the other. Therefore, the resultant matrix is fully populated, but small. On the other hand, volume methods are expected to have much more elements, because they discretize the entire volume. This means, there must be more potentials to be determined in volume methods. Nevertheless, volume methods couple each potential at every element only to its nearest neighbor and this makes the resultant matrix sparse, but still large [20].

Use of BEM for numerical solution of ECG problems has been very popular for more than four decades [21, 22, 23, 25]. The popularity of BEM mainly comes from the easiness of setting the problem and sufficiency for solving inhomogeneous regions of the torso. Although BEM provides quick and easy set up for numerical computations by using only two dimensional surface elements compared to volume methods which include three dimensional volume elements, it is not able to model cardiac anisotropy which has high effects on the resultant ECG with BEM. If the solution domain contains varying anisotropy and complexity, then volume methods are usually preferred for the numerical computation.

There are three types of volume methods namely finite difference method (FDM), finite element method (FEM), and finite volume method (FVM) [26, 20, 24, 25]. All of these methods have both merits and restrictions, which will be shortly explained below.

FDM uses regularly spaced three-dimensional array of nodes, which are connected to each other with resistors that represent torso resistances. For each connected node,

Kirchhoff's current law is used. As a result, large set of equations is formed to relate the potentials at neighboring nodes to each other. The accuracy of the solution is directly dependent on the node spacing and resistors that represent torso. Like other volume methods, FDM is also capable of solving anisotropic regions in a solution domain. The main disadvantage of FDM is its slow convergence [26].

FEM is another widely used volume method. It uses three-dimensional tetrahedral or hexahedral elements to subdivide the solution domain into simpler parts called as finite elements [20]. The main advantages of using finite elements are their ability to represent complex geometries such as geometries with irregular boundaries and dissimilar properties of materials in the solution domain accurately [26, 20, 24, 25]. However, there are also some disadvantages of FEM. FEM has element dependent solution that means the choice of shape quality and density of elements affect the solution. Therefore, during modeling with FEM, these parameters should be considered carefully. Also, due to the entire volume modeling, element number increases and thus complexity in computation rises. By using some adaptive solution methods, this handicap can be removed. A solution domain may include regions that need either fine or coarse solution. Hence, while fine solution needed region is modeled with high number of elements, coarse solution needed region can be modeled with less number of elements. Therefore, computational cost can be reduced [24].

FEM uses both element and node information in order to construct the shape functions needed for the solution. There is also another type of FEM, which uses only node and boundary information. This type of FEM is called as meshless FEM [27]. As the name implies, meshless FEM does not require meshing the solution domain, which is a time-consuming process. Recent studies have showed that meshless FEM has better convergence and less relative error than traditional FEM at the same node distribution. However, modeling inhomogeneous and anisotropic regions is not straightforward with meshless FEM. Also, computational load of meshless FEM is heavier than traditional FEM, because meshless FEM is not able to express shape functions [28].

The small volume surrounding each node in a discretized geometry is represented by FVM. FVM is based on integral equations and similar to FDM and FEM in terms of calculating the values at discrete mesh locations. In FVM, like other volume methods

the accuracy is dependent on density of the discretization. As a result of applying FVM, there occur many equations to represent the potentials at the centre of all volume elements [29].

2.4.1 Related Studies of the Forward Problem in Literature

In ECG problems, according to equivalent source definition and conductivity properties of the solution domain, either surface methods, volume methods or both surface and volume methods are applied. Surface method BEM is quite common solution method for ECG problems [30, 31, 32]. The main reasons which make BEM preferable are both its sufficiency to model the solution domain with small number of surface elements and its applicability to the regions with major inhomojenities in torso [21]. Also, use of small number of elements makes computational time with BEM modeling faster than the volume methods [33]. However, BEM is unable to deal with the anisotropic electrical conductivity of the interstitial space within the cardiac tissue, therefore researchers neglect anisotropy of both intra and extracellular spaces or only extracellular space [21]. Another disadvantage of BEM is its large amount of memory requirements [34]. EP, EDL models and dipole source representation of TMPs within the myocardium are the cardiac sources which are generally used for ECG forward problem studies with BEM [35, 36]. Since EP and EDL represent the electrical activity on the surface of the cardiac tissue, the anisotropy within the myocardium can be neglected. However, at some studies where dipole source representation is used, the inhomogeneous intracellular anisotropy is taken into consideration by using oblique dipole model [37].

For ECG forward problem studies, volume methods have recently gained importance for their convenience with anisotropic modeling. Solution of ECG forward problems by using FDM was first introduced by Walker and Kilpatrick in 1987 [20], but due to its slow convergence rate, FDM is used seldomly by the researchers [38, 26]. Another volume method, FVM was first applied to bioelectric problems in 1994 by Abboud et al. [20] and is similar to FEM. In literature, there are some applications of FVM to ECG problems[39]. Among volume methods, FEM is the most widely used one. Several groups utilize FEM in ECG problems with the availability of large amount

of FEM packages [40, 41, 42, 43, 44, 45, 46, 47, 48, 49, 50]. Since the anisotropic modeling of the cardiac tissue has very significant effects on the forward ECG problems, FEM modeling of the myocardium with its anisotropic electrical conductivity properties is very important [51]. A forward ECG study performed by Pilkington et al. in 1985 has showed that the accuracy of the ECG signal is higher and the solution is less sensitive when FEM is applied [52]. Another significant advantage of FEM in contrast to BEM, TMP distribution within the myocardium can be taken as equivalent cardiac source and other equivalent cardiac sources such as EP, EDL and equivalent dipole sources can be obtained from the equivalent TMP distributions within the myocardium.

In order to reduce computational complexity, some researchers apply surface and volume methods together. While anisotropic regions in the solution domain are modeled with FEM, isotropic regions are modeled with BEM. This approach was first applied to ECG problems by Stanley and Pilkington (1989) [20]. There are also other heart torso coupling studies with different numerical methods [53].

Nowadays, TMP has become a widely studied source model for both forward and inverse ECG studies [54, 55, 56, 57, 58, 59, 60]. Since TMP is the main source of cardiac action potential generation, compared to other source models TMP gives more detailed information about the electrical activity within the myocardium. Therefore, for inverse ECG studies TMP based transfer matrices have gained importance. Another significant advantage of using TMP is the linear representation of the problem. However, it has a very serious limitation, the solution is non-unique so the obtained solution may not be physiologically meaningful unless additional constraints are used [54]. Also the increase in problem size is a serious disadvantage which increases the computational cost.

2.5 Formulation of the Forward Problem

The problem of electrocardiography is governed by Maxwell's equations [1] :

$$\nabla \times E + \frac{\partial B}{\partial t} = 0 \tag{2.2}$$

$$\nabla \times H - \frac{\partial D}{\partial t} = J \tag{2.3}$$

In equations 2.2 and 2.3, E represents the electric field intensity, B represents the magnetic induction, H represents the magnetic field intensity, D represents the electric displacement and J represents the current density [1].

Since the measured electrocardiogram (ECG) from a patient does not contain frequencies above 1kHz, the impedance of the torso can be approximated as purely resistive and phase shift due to bioelectric field is ignored. Also, inductive, capacitive and propagation effects of biological tissues are neglected when their properties are considered.Therefore, problem becomes quasi-stationary that means torso is approximated as a passive volume conductor [5].

By taking quasi-static assumptions into account, the following time dependent terms of the equations 2.2 and 2.3 are neglected:

$$\frac{\partial B}{\partial t} = 0 \qquad \frac{\partial D}{\partial t} = 0 \tag{2.4}$$

The current density J is equal to the sum of any impressed source current density J_i and any conductive currents σE:

$$J = \sigma E + J_i \tag{2.5}$$

By taking divergence of both sides in Equation 2.5 and using J is solenoidal, Equation 2.6 is written:

$$\nabla \cdot J = \nabla \cdot (\sigma E + J_i) = 0 \tag{2.6}$$

By applying quasi-static assumptions Equation 2.2 becomes:

$$\nabla \times E = 0 \tag{2.7}$$

Since electric field E is conservative, E in equation 2.7 can be written as:

$$E = -\nabla\phi \tag{2.8}$$

ϕ is electric potential scalar that satisfies equation 2.7.

Finally, if equation 2.8 is substituted into equation 2.6, Poisson equation in an inhomogeneous body is obtained:

$$\nabla.(\sigma\nabla\phi) = \nabla.J_i = -I_{s,v} \tag{2.9}$$

$I_{s,v}$ is the current source in that volume conductor.

2.5.1 Bidomain Model

Bidomain model is an approximation that helps to examine cellular electrophysiology of the cardiac tissue which is composed of intra- and extracellular domains macroscopically [3]. Each of these domains possesses its own conductivity tensor and potential distribution. The following equations 2.10 and 2.11 represent the features of the intra- and extracellular domains [5] :

$$\nabla \cdot (\sigma_i \nabla\phi_i) = \beta I_m \tag{2.10}$$

$$\nabla \cdot (\sigma_e \nabla\phi_e) = -\beta I_m \tag{2.11}$$

where σ_i-ϕ_i and σ_e-ϕ_e are the conductivities-potentials of the intracellular and extracellular domains, respectively. β is the membrane surface to volume ratio and I_m is the transmembrane current density [5]. Since there is anisotropy in the cardiac tissue, the conductivities are in tensor forms as shown in the following equations 2.12 and

2.13.

$$\sigma_i = \begin{bmatrix} \sigma_{i,l} & 0 & 0 \\ 0 & \sigma_{i,t} & 0 \\ 0 & 0 & \sigma_{i,t} \end{bmatrix} \tag{2.12}$$

$$\sigma_e = \begin{bmatrix} \sigma_{e,l} & 0 & 0 \\ 0 & \sigma_{e,t} & 0 \\ 0 & 0 & \sigma_{e,t} \end{bmatrix} \tag{2.13}$$

where $\sigma_{i,l}$-$\sigma_{e,l}$ denotes intracellular and extracellular longitudinal conductivities (along the fiber direction) and $\sigma_{i,t}$-$\sigma_{e,t}$ denotes intracellular and extracellular transversal conductivities (perpendicular to the fiber direction). In order to obtain the Poisson's equation which represents the cardiac sources and the torso potentials in a macroscopic cellular electrophysiological level, we add equations 2.10 and 2.11 by considering $\phi_i = \phi_e + \phi_m$ and get the following equation [5]:

$$\nabla \cdot ((\sigma_i + \sigma_e)\nabla\phi_e) = -\nabla \cdot (\sigma_i \nabla \phi_m) \tag{2.14}$$

CHAPTER 3

MODELING OF THE FORWARD PROBLEM

3.1 Governing Equations and Boundary Conditions

The electrical activity between the myocardium and the body surface is modeled by the following equations [1]:

$$\nabla \cdot ((\sigma_i + \sigma_e)\nabla\phi_e) = -\nabla \cdot (\sigma_i \nabla\phi_m) \qquad in \qquad \Omega_H \tag{3.1}$$

$$\nabla \cdot (\sigma_o \nabla\phi_o) = 0 \qquad in \qquad \Omega_T \tag{3.2}$$

Equation 3.1 is the bidomain model based Poisson equation and gives the relation between the cardiac sources generated by the TMPs (ϕ_m where $\phi_m = \phi_i - \phi_e$) and the extracellular potentials (ϕ_e) within the heart. As described previously, bidomain model represents groups of cells within the myocardium as discrete points by taking a continuous approach. Equation 3.2 is the reduced form of the Equation 3.1 for the regions where there is no source is defined. In this equation ϕ_o represents extracellular potential distribution within the torso. Ω_H and Ω_T represent finite volume of the volume conductor for heart and torso respectively (see Figure 3.1). This volume conductor consists of two boundaries; Γ_H represents heart surface and Γ_T represents torso surface. Electrical conductivity of torso which surrounds the volume conductor that represents the heart is denoted by σ_o and electrical conductivities of intracellular and extracellular domains in the heart are represented as σ_i and σ_e. Torso is surrounded by air which has $\sigma = 0$. Considering Figure 3.1 these two equations can be explained better with the following boundary conditions [29]:

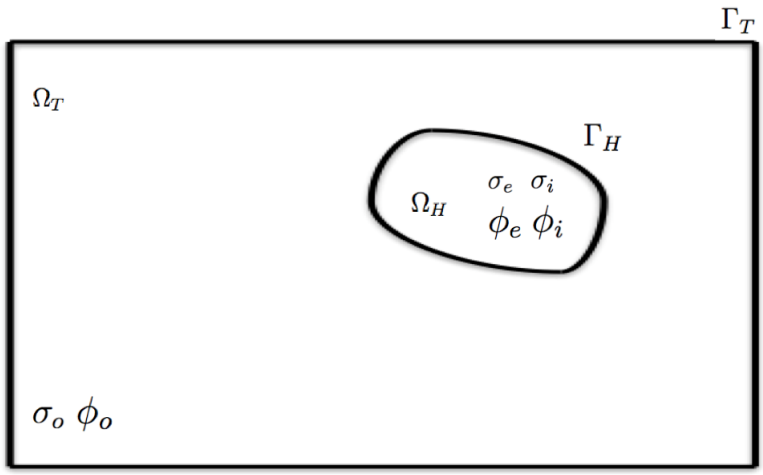

Figure 3.1: Simple heart and torso model in 2D

$$\phi_e = \phi_o \qquad on \qquad \Gamma_H \tag{3.3}$$

$$\sigma_i \frac{\partial \phi_i}{\partial n} + \sigma_e \frac{\partial \phi_e}{\partial n} = \sigma_o \frac{\partial \phi_o}{\partial n} \qquad on \qquad \Gamma_H \tag{3.4}$$

$$\sigma_i \frac{\partial \phi_i}{\partial n} = 0 \qquad on \qquad \Gamma_H \tag{3.5}$$

$$\sigma_o \frac{\partial \phi_o}{\partial n} = 0 \qquad on \qquad \Gamma_T \tag{3.6}$$

Equation 3.3 and 3.4 denotes continuity of intracellular potentials and total current within the heart across the heart-torso interface (Γ_H), and Equation 3.5 ensures that intracellular current can not exceed heart-torso interface (Γ_H). The last boundary condition given by Equation 3.6 specifies that extracellular current inside the torso vanishes at torso-air interface (Γ_T).

3.2 Transfer Matrix for Transmembrane Potentials

Solution of the forward problem yields a transfer matrix which contains information about electrical conductivity and geometry of a volume conductor. Depending on the choice of equivalent cardiac sources, there exist different solution methods for the transfer matrix computation [5]. In this study, equivalent cardiac sources are taken as TMPs. Since there is a linear relationship between the TMPs within the heart and the

corresponding extracellular potentials, Equations 3.1 and 3.2 can be reduced into the following matrix equation form:

$$T\phi_m = \phi_e \tag{3.7}$$

In Equation 3.7, ϕ_m is directly linked to the ϕ_e and transfer matrix is defined as T. In this equation, it is important to note that ϕ_m and ϕ_e represent potentials in a discrete manner instead of continuous approach.

3.2.1 Point Cloud Modeling

In reality, there are thousands of cardiac cells and each of them has its own TMP. Since it is impossible to model the real case, transfer matrix is obtained by investigating cardiac tissue at macroscopic level (bidomain model). By this way, TMP distribution on the cardiac tissue can be modeled as specific number of points and then transfer matrix could be obtained.

Following the method in [5], each of the TMPs on the cardiac tissue is set to unity in sequence and TMPs of the remaining cells to zeros. Each time that one of the TMPs from point cloud is set to unity, measuring the extracellular potentials on the torso from fixed coordinates will give each column of the transfer matrix, T. By repeating this procedure for all of the points that represent the TMPs on the cardiac tissue, T can be computed entirely. In order to explain this approach in a better way, by assuming nine cardiac cells within the heart the following Equations 3.8, 3.9 and 3.10 can be written:

$$\begin{bmatrix} \phi_e^1 \\ \phi_e^2 \\ \phi_e^3 \end{bmatrix}_{3\times1} = \begin{bmatrix} \vdots & \vdots & \cdots & \vdots \\ t_1 & t_2 & \cdots & t_9 \\ \vdots & \vdots & \cdots & \vdots \end{bmatrix}_{3\times9} \begin{bmatrix} \phi_m(1) \\ \phi_m(2) \\ \vdots \\ \phi_m(9) \end{bmatrix}_{9\times1} \tag{3.8}$$

$$\begin{bmatrix} \phi_e^1 \\ \phi_e^2 \\ \phi_e^3 \end{bmatrix} = \phi_m(1) \begin{bmatrix} \vdots \\ t_1 \\ \vdots \end{bmatrix} + \phi_m(2) \begin{bmatrix} \vdots \\ t_2 \\ \vdots \end{bmatrix} + \ldots + \phi_m(9) \begin{bmatrix} \vdots \\ t_9 \\ \vdots \end{bmatrix} \tag{3.9}$$

If $\phi_m(1) = 1$ and for $i = 2 : 9$ $\phi_m(i) = 0$, then;

$$\begin{bmatrix} \phi_e^1 \\ \phi_e^2 \\ \phi_e^3 \end{bmatrix} = \begin{bmatrix} \vdots \\ t_1 \\ \vdots \end{bmatrix} \tag{3.10}$$

From these Equations, it can easily be observed that for each ϕ_m set to unity, one of the columns of the transfer matrix T is obtained.

3.3 Test Problem

In order to understand the behavior of the electrocardiographic problems, analytical solutions to mathematical problems have been used. Although numerical solution methods are better to use for complex real world problems, they contain some modeling errors [61]. Therefore, it is necessary to verify the results of these numerical solutions with analytical solutions.

Although numerical solutions are defined in cartesian coordinate system, the analytical solution for the problem set up in Figure 3.2 is derived in spherical polar coordinate system with coordinates (r, θ, ζ). Here, θ represents the circumferential angle with $0 \leq \theta \leq 2\pi$ and ζ represents the azimuthal angle with $0 \leq \zeta \leq \pi$.

3.3.1 Analytical Solution

The electrical activity inside of the inner sphere which represents the myocardium is modeled by the Poisson Equation which is described previously. Since there is no current source coming externally to the region outside of the heart (the region between the inner and the outer spheres in Figure 3.2), the Poisson equation (Equation 3.11)

reduces to a generalized Laplace's Equation (Equation 3.12).

Figure 3.2 is a simple concentric sphere set up for analytical solution of this problem. In this set up, σ_i and σ_e are the intracellular and extracellular conductivities of the inner sphere respectively and σ is the passive conductivity of the outer sphere. Extracellular potential within the heart is given by ϕ_e^{in} and the extracellular potential within the torso is defined between the inner and outer spheres with radii R_1 and R_2 respectively is given by ϕ_e^{out}.

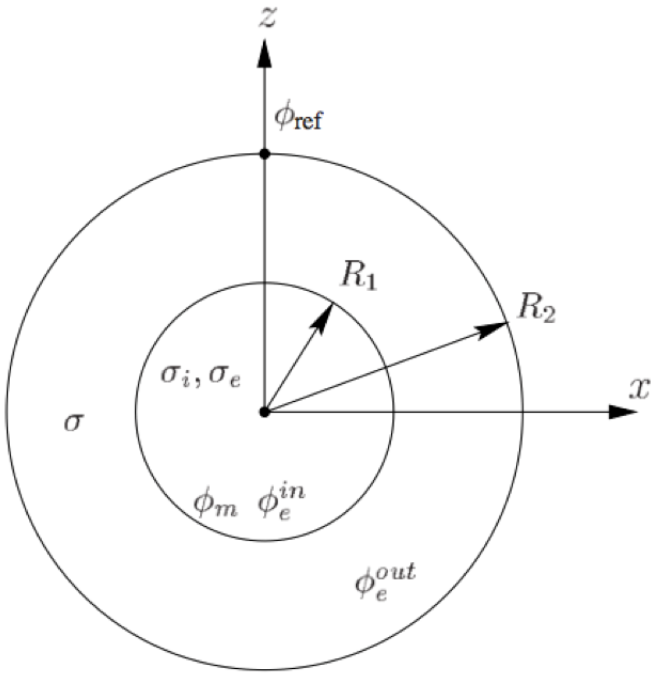

Figure 3.2: Schematic of bidomain problem set up with inner sphere of radius R_1 and outer sphere of radius R_2 [1]

$$\nabla \cdot ((\sigma_i + \sigma_e)\nabla \phi_e^{in}) = -\nabla \cdot (\sigma_i \nabla \phi_m) \qquad in \qquad 0 < r \leq R_1 \tag{3.11}$$

$$\nabla \cdot (\sigma \nabla \phi_e^{out}) = 0 \qquad in \qquad R_1 < r \leq R_2 \tag{3.12}$$

Both Equations 3.11 and 3.12 define a boundary value problem, together with the following boundary conditions:

$$\phi_e^{out} = \phi_e^{in} \qquad at \qquad r = R_1 \tag{3.13}$$

$$(\sigma_i + \sigma_e)\frac{\partial \phi_e^{in}}{\partial r} = (\sigma)\frac{\partial \phi_e^{out}}{\partial r} \qquad at \qquad r = R_1 \tag{3.14}$$

$$\frac{\partial \phi_e^{out}}{\partial r} = 0 \qquad at \qquad r = R_2 \tag{3.15}$$

$$\phi_e^{out} = 0 \qquad at \qquad r = R_2, \qquad \zeta = 0, \qquad \theta = 0 \tag{3.16}$$

As specified by first and second boundary conditions, equivalence of the extracellular potentials (ϕ_e^{in} and ϕ_e^{out}) and continuity of current across the boundary between the inner and the outer spheres are given by Equations 3.13 and 3.14 respectively. The third boundary condition given by 3.15 ensures that there is electrical insulation for ϕ_e^{out} on heart torso surface. Additionally, Equation 3.16 shows the reference potential boundary condition.

For the region inside of the inner sphere which represents the heart domain (Figure 3.2), Equation 3.11 can be written in the following Laplace's equation form when inner region is assumed to be homogeneous and isotropic:

$$\nabla^2(\phi_e^{in} + \frac{\sigma_i}{\sigma_i + \sigma_e}\phi_m) = 0 \tag{3.17}$$

The general analytical solution to Laplace's equation in spherical coordinates is given by Equation 3.18. In this equation $P_m^n(\cos\zeta)$ is the associate Legendre Polynomial. Due to the orthogonality of spherical harmonic functions, mn terms only contain 00, 01 and 11 coefficients [1].

$$\phi = \sum_{n=0}^{\infty}\sum_{m=0}^{n}(A_{mn}\cos(m\theta) + B_{mn}\sin(m\theta))(C_{mn}r^n + \frac{D_{mn}}{r^{n+1}})P_n^m(\cos\zeta) \tag{3.18}$$

If there are more than one solution to Laplace's equations in the related problem, Equation 3.18 can also be written with different coefficients:

$$\phi = \sum_{n=0}^{\infty}\sum_{m=0}^{n}(E_{mn}\cos(m\theta) + F_{mn}\sin(m\theta))(G_{mn}r^n + \frac{H_{mn}}{r^{n+1}})P_n^m(\cos\zeta) \tag{3.19}$$

By defining ϕ_m as the potential field generated by a centric current dipole source and considering electrical insulation on the surface of the inner sphere, the following analytical TMP equation in spherical polar coordinate system is derived [1]:

$$\phi_m(r,\theta,\zeta) = \frac{(R_1^3 + 2r^3)}{(R_1^3 r^2)}(p_x \cos\theta \sin\zeta + p_y \sin\theta \sin\zeta + p_z \cos\zeta) \tag{3.20}$$

Note that, centric dipole is defined in the cartesian coordinate system with a moment of $p = (p_x, p_y, p_z)$ inside a sphere of radius R_1.

If ϕ_m is a solution of Laplace's equation 3.17, then the analytic derivation of ϕ_e^{in} which satisfies Equation 3.17 can also be obtained:

$$\begin{aligned}\phi_e^{in}(r,\theta,\zeta) = (A_{11}\cos\theta + B_{11}\sin\theta)(C_{11}r + \frac{D_{11}}{r^2})\sin\zeta + (C_1 r + \frac{D_1}{r^2})\cos\zeta \\ + C_0 + \frac{D_0}{r} - \frac{\sigma_i}{\sigma_i + \sigma_e}\phi_m(r,\theta,\zeta)\end{aligned} \tag{3.21}$$

By interpreting 3.12 and applying the same procedure described above, the following analytical solution for ϕ_e^{out} is written as:

$$\begin{aligned}\phi_e^{out}(r,\theta,\zeta) = (E_{11}\cos\theta + F_{11}\sin\theta)(G_{11}r + \frac{H_{11}}{r^2})\sin\zeta + (G_1 r + \frac{H_1}{r^2})\cos\zeta \\ + G_0 + \frac{H_0}{r}\end{aligned} \tag{3.22}$$

In order to find solutions to these analytical extracellular potentials for a given specific dipole source, first of all the coefficients in the Equations 3.21 and 3.22 must be calculated.

If Equations 3.21 and 3.22 are equated to each other by taking into account the continuity of potentials across the surface of the inner sphere implied by the boundary condition 3.13, the following equations which show the relations between the coefficients are derived :

$$G_0 + \frac{H_0}{R_1} = C_0 + \frac{D_0}{R_1} \tag{3.23}$$

$$E_{11}(G_{11}R_1 + \frac{H_{11}}{R_1^2}) = A_{11}(C_{11}R_1 + \frac{D_{11}}{R_1^2}) - \frac{3\sigma_i}{R_1^2(\sigma_i + \sigma_e)}p_x \tag{3.24}$$

$$F_{11}(G_{11}R_1 + \frac{H_{11}}{R_1^2}) = B_{11}(C_{11}R_1 + \frac{D_{11}}{R_1^2}) - \frac{3\sigma_i}{R_1^2(\sigma_i + \sigma_e)}p_y \tag{3.25}$$

$$G_1R_1 + \frac{H_1}{R_1^2} = C_1R_1 + \frac{D_1}{R_1^2} - \frac{3\sigma_i}{R_1^2(\sigma_i + \sigma_e)}p_z \tag{3.26}$$

Continuity of current across the surface of the inner surface is defined by the boundary condition 3.14. By taking derivatives of both ϕ_e^{in} and ϕ_e^{out} with respect to r and equating them to each other by using Equation 3.14, the following equations are obtained:

$$\sigma\frac{H_0}{R_1^2} = (\sigma_i + \sigma_e)\frac{D_0}{R_1^2} \tag{3.27}$$

$$\sigma E_{11}(G_{11} - \frac{2H_{11}}{R_1^3}) = (\sigma_i + \sigma_e)A_{11}(C_{11} - \frac{2D_{11}}{R_1^3}) \tag{3.28}$$

$$\sigma F_{11}(G_{11} - \frac{2H_{11}}{R_1^3}) = (\sigma_i + \sigma_e)B_{11}(C_{11} - \frac{2D_{11}}{R_1^3}) \tag{3.29}$$

$$\sigma(G_1 - \frac{2H_1}{R_1^3}) = (\sigma_i + \sigma_e)(C_1 - \frac{2D_1}{R_1^3}) \tag{3.30}$$

Substituting ϕ_e^{out} into Equation 3.15 which is a no-flux boundary condition across the outer surface gives the following equation set:

$$G_{11} - \frac{2H_{11}}{R_2^3} = 0 \tag{3.31}$$

$$G_1 - \frac{2H_1}{R_2^3} = 0 \tag{3.32}$$

$$\frac{-H_0}{R_2^2} = 0 \tag{3.33}$$

Finally, Equation 3.34 is obtained by considering reference potential boundary condition given by Equation 3.16 and defining reference potential at coordinates $(R_2, \theta, 0)$:

$$\phi_{ref} = G_1 R_2 + \frac{H_1}{R_2^2} + G_0 + \frac{H_0}{R_2^2} \tag{3.34}$$

There are 12 Equations from Equations 3.23 to 3.34 and 16 unknowns (coefficients from A_{11} to H_{11} and coefficients C_0, C_1, D_0, D_1, G_0, G_1, H_0, H_1). Since the number of unknowns is more than the number of equations, the problem is underdetermined. In order to solve this problem, 4 coefficients must be fixed. To kill the singularity at the origin, the fixed coefficients must be chosen as $p = (A_{11}D_{11}, B_{11}D_{11}, D_1)$. That means coefficients D_{11} and H_{11} can be chosen as 1 or any positive integer and D_1 is fixed as given dipole moment in z direction. According to the selected D_{11} and H_{11} coefficients, A_{11} and B_{11} are also determined.

A particular solution for Equations 3.21 and 3.22 can be done by a specific dipole source with moment of $p = (1, 2, 1)\ (A.m)$ and conductivities $\sigma_i = 2\ (S/m)$, $\sigma_i = 2\ (S/m)$, $\sigma = 2\ (S/m)$ with radiuses $R_1 = 1\ (m)$ and $R_2 = 3\ (m)$ for the set up in Figure 3.2.

The fixed coefficients are:

$$D_{11} = 1 \qquad H_{11} = 1 \qquad D_1 = 1 \tag{3.35}$$

Therefore, other coefficients are calculated as:

$$A_{11} = 0.3333 \qquad H_0 = 0 \qquad D_0 = 0 \tag{3.36}$$

$$B_{11} = 0.6667 \qquad D_{11} = 1 \qquad E_{11} = 0.3885 \qquad F_{11} = 0.7770 \qquad G_{11} = 0.0741 \tag{3.37}$$

$$C_0 = -0.1295 \qquad D_1 = 0.3333 \qquad G_0 = -0.1295 \qquad G_1 = 0.0288 \qquad H_1 = 0.3885 \tag{3.38}$$

3.3.2 COMSOL Modeling with Dipole

In this study, numerical simulation environment is provided by COMSOL Multiphysics program which can automatically discretize the solution domain by using finite element method (FEM) [2]. First of all, the set up in Figure 3.2 with its governing equations and conductivity parameters is created and simulated in COMSOL, then the results of analytical solutions are compared with the results of numerical solutions.

The governing Equations 3.11 and 3.12 are derived in COMSOL by using Electric Currents Module which includes the following equations:

$$\nabla \cdot J = Q_j \tag{3.39}$$

$$E = -\nabla.\phi \tag{3.40}$$

$$J = \sigma E + J_e \tag{3.41}$$

In COMSOL simulation environment, 2 Studies and 2 Electric Currents Modules are added into the solution domain. In Study 1, Electric Currents 1 is simulated and in Study 2, Electric Currents 2 is simulated. Since there is no time dependency in the problem, both Study 1 and Study 2 are selected as stationary.

In Study 1, a dipole source with moment of $p = (1, 2, 1)$ is defined at the center of the inner sphere. This dipole source constitutes the current source Q_j given by Equation 3.39. Since there is no externally added current density J_e in the solution domain, the current density J due to the current source Q_j and by this way the electric field

E is calculated. Then, by using Equation 3.40, the potential distribution ϕ which is assumed to be the TMP distribution (ϕ_m) for this problem is obtained.

In Study 2, the current density J generated by ϕ_m is defined as source and called as external current density J_e from Study 1. Then, by applying same steps described in Study 1, extracellular potentials ϕ_e^{in} and ϕ_e^{out} located on both the inner and the outer spheres are calculated.

In COMSOL, The continuity of potential across the surface of the inner sphere is provided by finite elements and electrical insulation is defined by $n.J = 0$ that means the normal component of the current density is equal to zero on the surface of the outer sphere.

3.3.3 COMSOL Modeling with Point Cloud

As previously described, transfer matrix T is obtained by point cloud modeling. In COMSOL, point cloud modeling first starts by generating mesh in the solution domain. The nodes of this generated mesh is assumed as cardiac cells. Therefore, coordinates of these mesh nodes are extracted from COMSOL and used to describe the locations of the TMPs. The number of points in this model is specified by the mesh element size. Increase in the mesh element size means decrease in the number of nodes or vice versa.

After obtaining coordinates of the mesh nodes, point objects at these coordinates are builded inside of the inner sphere in COMSOL. Note that, the nodes on the surface of the sphere are extracted, because this region is assumed as epicardium and electrically inactive. Then, the procedure described in COMSOL Modeling with Dipole section is applied, but this time TMP distribution is directly used instead of generating from dipole source. Since the purpose of the point cloud modeling is to construct transfer matrix T, TMP distribution is composed of only unity and zeros. Detailed explanation about this method can be found in the previously explained Point Cloud Modeling section.

Although cardiac tissue is examined at macroscopic level in this study, there are still a lot of points to be builded in COMSOL for TMP representation. Therefore, it is very

difficult to make this geometrical modeling by using graphical user interface (GUI). Also, each time a point is set to unity while others zero, simulation including Study 1 and Study 2 must be repeated manually. In order to overcome these drawbacks of the point cloud modeling, COMSOL with MATLAB is preferred instead of GUI.

3.3.4 Verification

In this section, first of all numerical solution carried by COMSOL is verified with the analytical solution for transmembrane potentials (TMPs). Secondly, COMSOL point cloud modeling is compared with the analytical solution for extracellular potential ϕ_e in order to understand the accuracy of the constructed transfer matrix, T. To prevent confusion between the terms while presenting the results, analytical solutions are represented as ϕ_m^A and ϕ_e^A and numerical solutions are represented as ϕ_m^N for TMPs and ϕ_e^P for extracellular potentials obtained by point cloud modeling.

As previously explained, COMSOL uses finite element method (FEM). In FEM, changing mesh element size may have significant effect on the results. Therefore, mesh sensitivity analysis must firstly be done during numerical analysis by changing the mesh element size. Generally, numerical solution error is expected to become less by decreasing the size of the mesh elements (refinement of mesh).

In this study, mesh sensitivity analyses are done with five different mesh element sizes. Table 3.1 shows used maximum mesh element sizes (hmax) at spheres with radius R_1 and R_2. From this table it can be seen that both total mesh element number and degrees of freedom (DOF) increase by decreasing the mesh element size.

Table 3.1: Mesh properties with different mesh element sizes

Mesh Properties	**Mesh 1**	**Mesh 2**	**Mesh 3**
R_2 **hmax** (m)	0.4	0.4	0.2
R_1 **hmax** (m)	0.3	0.06	0.06
$\#$ **of elements**	14.2×10^4	43.6×10^4	62.9×10^4
DOF	$192K$	$585K$	$847K$

In order to understand how ϕ_m^N change with different mesh sizes, four symmetrically located points are selected from the set up created in COMSOL (Table 3.2) and their potentials are compared with analytical solutions by calculating percentage relative

error between them. The percentage relative error metric is given by Equation 3.42 where TV stands for True Value and AV stands for Approximate Value.

$$E = \frac{|TV - AV|}{|TV|} \times 100 \tag{3.42}$$

Table 3.2: Coordinates of the points in cartesian system

Points	**x**	**y**	**z**
Pt 1	0.5	0	0
Pt 2	0	0.5	0
Pt 3	-0.5	0	0
Pt 4	0	-0.5	0

Table 3.3 shows mesh sensitivity analysis for ϕ_m^N created by the dipole source at four different points located on the inner sphere. As can be observed from the table, with the refinement of mesh, numerical solution starts to converge and the relative error between ϕ_m^A and ϕ_m^N starts to become less. The converged plots of ϕ_m^N with ϕ_m^A for different θ and ζ combinations in the radial direction is shown in Figure 3.3 and the inner sphere volume distribution of ϕ_m^N generated by the dipole source in COMSOL is indicated by Figure 3.4.

Table 3.3: $\boldsymbol{\phi_m^N}$ (V) Mesh Sensitivity Sudy

		COMSOL		**COMSOL**		**COMSOL**	
		Mesh 1		**Mesh 2**		**Mesh 3**	
Points	$\boldsymbol{\phi_m^A(V)}$	$\boldsymbol{\phi_m^N(V)}$	**E**(%)	$\boldsymbol{\phi_m^N(V)}$	**E**(%)	$\boldsymbol{\phi_m^N(V)}$	**E**(%)
1	5	5.756	15.1	4.913	1.7	4.995	0.1
2	10	10.746	7.5	9.912	0.9	9.995	0.1
3	-5	-4.199	16.0	-5.087	1.7	-5.005	0.1
4	-10	-9.124	8.8	-10.086	0.9	-10.004	0.0

Secondly, the accuracy of transfer matrix T is analyzed. First of all, four cartesian point cloud combinations are generated with four different step sizes given by Table 3.4. Here, step sizes represent distances between the nodes in the point clouds. Therefore, decreasing step size causes an increase in the node numbers. After point cloud generation, T is constructed at mesh element sizes where numerical solution is converged (Table 3.1). Here, attention was paid to select the mesh element size of the inner sphere with R_1 where points are located so that it will divide the distance between the nodes to at least five. Number of nodes and mesh element size are main

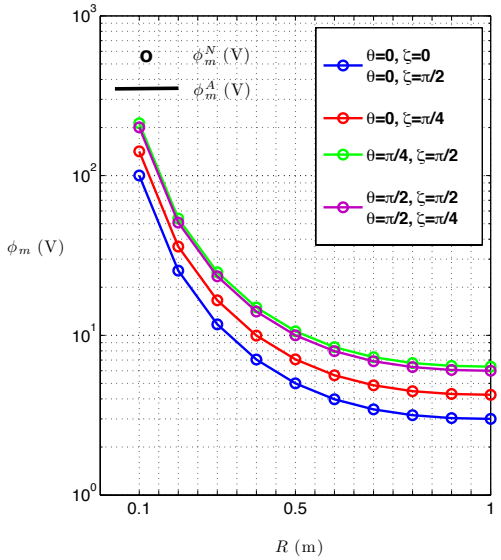

Figure 3.3: ϕ_m^A (V) and converged ϕ_m^N (V) plots for different θ and ζ combinations in the radial direction.

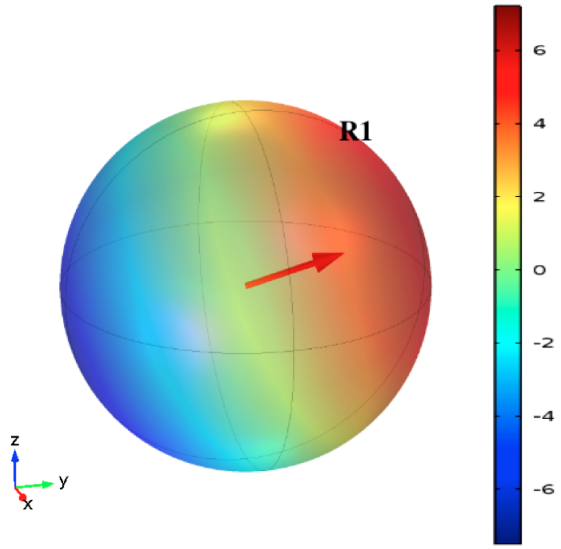

Figure 3.4: ϕ_m^N (V) distribution inside of the inner sphere with radius R_1 (m) in COMSOL. The arrow represents the polarization of the dipole source $p = (1, 2, 1)$ (A.m)

factors affecting the computational costs. Therefore, for the studies where results show convergence at very small mesh element sizes with high number of nodes, it is really difficult to obtain T with today's computer technology.

Table 3.4: # of Nodes Generated with Different Step Sizes

Step Size (m)	**Node #**
0.4	87
0.3	145
0.25	250
0.2	460

Column numbers of T are identified by the number of nodes in the point cloud and row numbers of T are identified by the fixed potential measurement locations on the surface of the outer sphere. In this study, T is constructed from 76 fixed measurement points located on the outer sphere surface for four point cloud combinations given by Table 3.4. Then by using Equation 3.7, $[\phi_e^P]$ values are obtained by multiplying the constructed T for each point cloud with $[\phi_m^A]$ calculated at corresponding point cloud coordinates. The following equations gives $[\phi_e^P]$ values for each point cloud :

$$[T]_{76\times87}[\phi_m^A]_{87\times1} = [\phi_e^P]_{76\times1} \tag{3.43}$$

$$[T]_{76\times145}[\phi_m^A]_{145\times1} = [\phi_e^P]_{76\times1} \tag{3.44}$$

$$[T]_{76\times250}[\phi_m^A]_{250\times1} = [\phi_e^P]_{76\times1} \tag{3.45}$$

$$[T]_{76\times460}[\phi_m^A]_{460\times1} = [\phi_e^P]_{76\times1} \tag{3.46}$$

Table 3.5 gives the accuracy of constructed T by comparing $[\phi_e^P]_{76\times1}$ and $[\phi_e^A]_{76\times1}$ according to point cloud combinations with average relative error between them. T is constructed at four different point clouds and each ϕ_e^P obtained from each T is compared with ϕ_e^A.

Table 3.5: Error between $[\phi_e^P]_{76\times1}$ and $[\phi_e^A]_{76\times1}$ at different point clouds

# of Nodes	**Error%**
87	38
145	27
250	19
460	0.4

From Table 3.5, it can easily be observed that with an increase in node numbers of point cloud, the relative error between $[\phi_e^P]_{76\times1}$ and $[\phi_e^A]_{76\times1}$ decreases or vice versa. Therefore, it can be said that constructed T with 460 points has the minimum error value while T with 87 points has the maximum.

Figure 3.5 and Figure 3.6 shows the worst and the best case scenarios of Table 3.5 by comparing $[\phi_e^P]_{76\times1}$ and $[\phi_e^A]_{76\times1}$ values measured from 76 different locations on the surface of the outer sphere (R_2) with varying θ and ζ angles. Results has showed convergence at extracellular potentials ϕ_e obtained from T constructed with 460 nodes. That means point cloud generated with 460 nodes is the lowest limit to define ϕ_m distribution generated by dipole source exactly. If node numbers are taken higher than 460 nodes by decreasing step size, the new results are expected to be same with the analytical solution. However, here the important point is to construct new T with an appropriate mesh to get the most accurate interpolation of TMPs. That means, as explained before highest mesh element size must be selected at mesh size where numerical solution is mesh independent anymore. Also, the selected mesh size of the inner sphere with R_1 must divide the distance between the nodes to at least five mesh elements. Note that decrease in mesh element size with an increased number of nodes in a point cloud will cause a rise in computational cost.

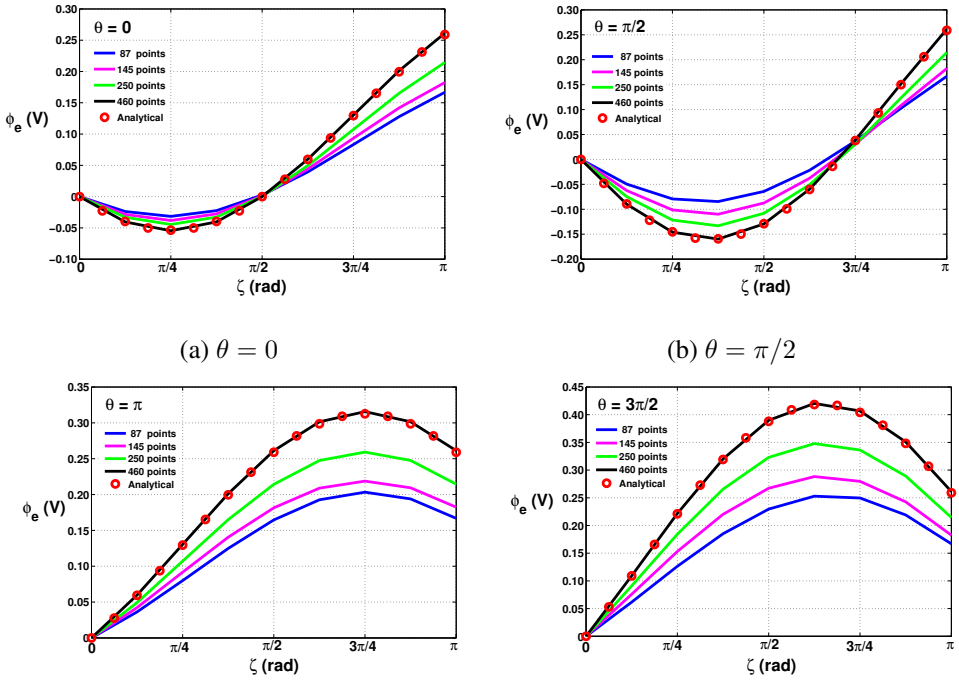

(a) $\theta = 0$ (b) $\theta = \pi/2$

(c) $\theta = \pi$ (d) $\theta = 3\pi/2$

Figure 3.5: $\phi_e^A\ (V)$ and $\phi_e^P\ (V)$ plots for varying θ and ζ angles with different point clouds

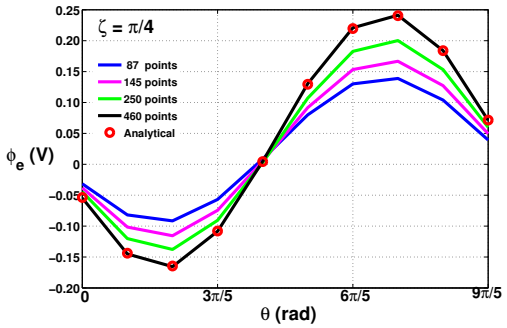

(a) $\zeta = \pi/4$

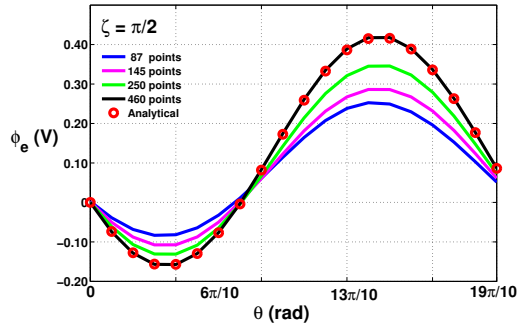

(b) $\zeta = \pi/2$

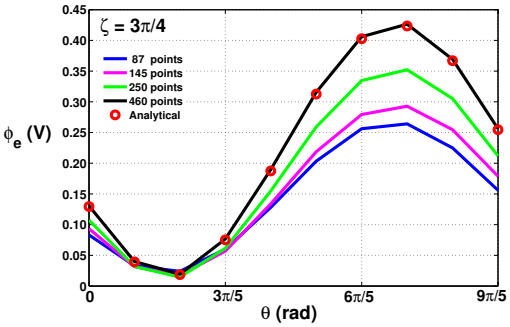

(c) $\zeta = 3\pi/4$

Figure 3.6: $\phi_e^A\ (V)$ and $\phi_e^P\ (V)$ plots for varying θ and ζ angles with different point clouds

CHAPTER 4

POINT CLOUD MODELING OF SPHERICAL HEART WITH IRREGULAR TORSO

In this chapter, COMSOL point cloud modeling has been applied to irregular torso geometry with spherical heart as shown in Figure 4.1. Due to lack of realistic TMP data for generic heart model, simulations are done by using sphere instead of heart and dipole source for TMP generation. The purpose of this chapter is to show the applicability of point cloud modeling to any irregular geometry.

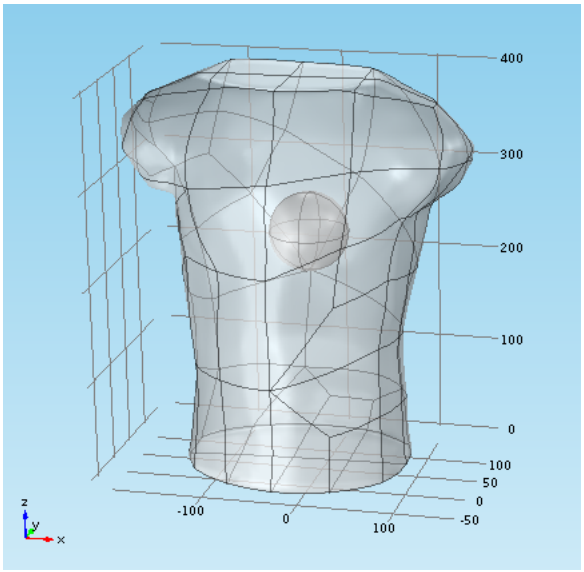

Figure 4.1: Realistic torso with spherical heart of R=40 mm.

As explained in Chapter 2, ECG QRS waveform is generated during the epicardial depolarization and repolarization of the ventricles. Since there is no TMP data to represent each time instants of real ECG waveform, simulations are done by using a dipole source which mimics epicardial potential distribution during ventricular de-

polarization. To show the accuracy of transfer matrix T constructed by point cloud modeling, body surface potential values coming from direct forward simulation are compared with body surface potentials obtained by T. Torso potential measurement locations are selected as in Figure 4.2. RA, LA, LL are the potential locations in which traditional limb leads (lead I, lead II, lead III) are derived from and V1-V6 are unipolar chest leads on horizontal torso plane. G stands for ground.

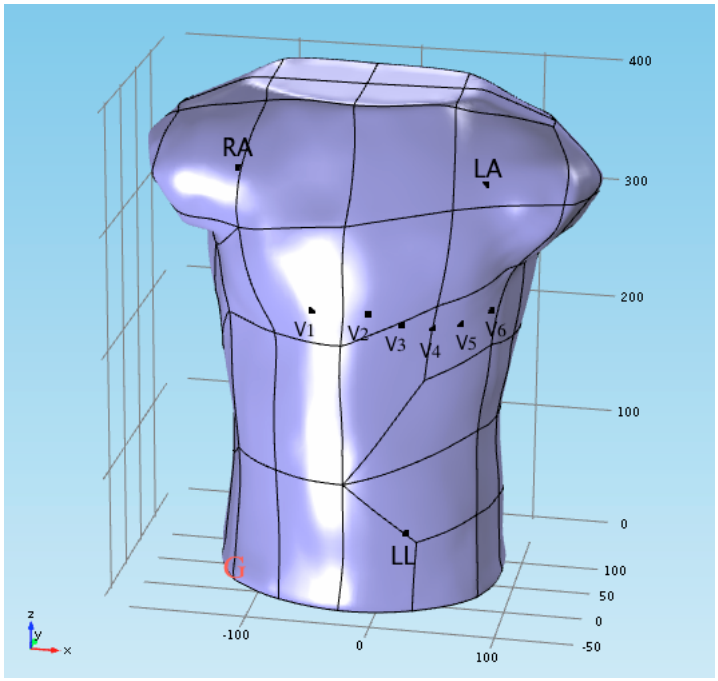

Figure 4.2: Body surface potential measurement locations.

An electric dipole source with moment of $p = (-0.02, 0.02, 0.02)\ (A.m)$ is located at the center of the sphere and conductivities are selected as σ_i=200 (S/m), σ_e=300 (S/m), σ=200 (S/m). The x, y and z coordinates of dipole moment is selected experimentally in a way that will mimic the ventricular depolarization. Note that the TMP distribution generated by this dipole source does not reflect the realistic distribution.

First of all, mesh sensitivity analysis are done for both ϕ_m^N and ϕ_e^N with five different mesh element sizes given in Table 4.1. For ϕ_m^N, four symmetrically located points are specified inside of the sphere in Figure 4.3 and change in their potentials are examined for each different mesh sizes. In Table 4.3, the change in ϕ_m^N values with the refinement of mesh from Mesh 1 to Mesh 4 can be examined better. While there is a difference between the ϕ_m^N values at Mesh 1 and Mesh 2, the potential values start

to show stability at Mesh 3 and Mesh 4 with very small changes between each other. That means the solution for ϕ_m^N starts to converge at Mesh 3.

Table 4.1: Different Mesh Properties

Mesh	**hmax** (mm)	**# of Elements**
Mesh 1	40	2.1×10^3
Mesh 2	20	2.2×10^3
Mesh 3	15	2.3×10^3
Mesh 4	8	3.6×10^3

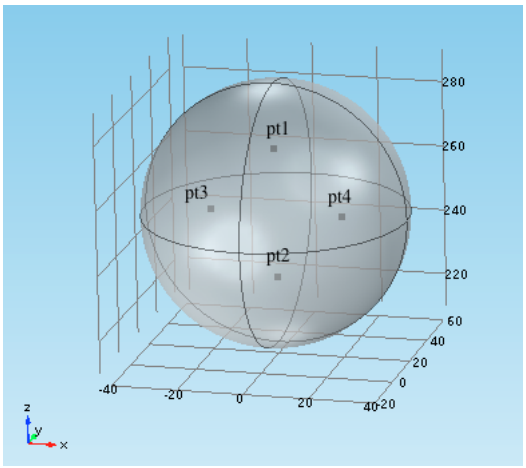

Figure 4.3: Point locations for ϕ_m^N calculation inside of sphere with R=40 mm.

Table 4.2: Coordinates of the points given in Figure 4.3 in cartesian system

Points	**x**	**y**	**z**
Pt 1	0	20	270
Pt 2	0	20	230
Pt 3	-20	20	250
Pt 4	20	20	250

Table 4.3: $\boldsymbol{\phi_m^N}$ Mesh Sensitivity Sudy

	$\boldsymbol{\phi_m^N}$ $(\boldsymbol{mV})$			
Points	**Mesh 1**	**Mesh 2**	**Mesh 3**	**Mesh 4**
1	16.38	26.93	23.81	24.16
2	-59.99	-33.79	-26.90	-25.22
3	51.89	21.42	23.87	24.45
4	-29.78	-26.05	-24.61	-25.58

Secondly, mesh sensitivity analysis are done for ϕ_e^N from the body surface measurement locations based on 12 Lead ECG system (Figure 4.2). By using this measurement locations, the aim is to show that point cloud modeling gives the same poten-

tial distribution with the direct forward simulations at the critical points where ECG waveform is generated from. In Table 4.4, ϕ_e^N values from Mesh 1 to Mesh 4 are given. Since the torso measurement points are not located nearly to the source coming from the sphere, ϕ_e^N values does not show significant changes with the refinement of mesh. This means the ϕ_e^N values at these locations show convergence at higher mesh element sizes. Figure 4.4 shows ϕ_e^N distribution on torso during complete depolarization of both ventricles at converged solution for ϕ_e^N (Mesh 3).

Table 4.4: $\boldsymbol{\phi_e^N}$ Mesh Sensitivity Sudy

	$\boldsymbol{\phi_e^N}$ $(\boldsymbol{mV})$			
Points	**Mesh 1**	**Mesh 2**	**Mesh 3**	**Mesh 4**
RA	-1.06	-1.06	-1.06	-1.06
LA	-0.13	-0.13	-0.12	-0.12
LL	0.89	0.89	0.89	0.89
V1	0.50	0.48	0.49	0.49
V2	1.74	1.75	1.75	1.75
V3	2.65	2.63	2.63	2.63
V4	2.99	2.96	2.96	2.96
V5	2.65	2.65	2.64	2.64
V6	1.91	1.91	1.90	1.90

Point cloud generation of this chapter differs from Chapter 3. In this chapter, first of all a coarse mesh is generated on the geometry which represents the heart. Then, node coordinates of this mesh is extracted and T matrix is constructed. While generating coarse mesh on sphere with radius $R = 40(mm)$, the following three point clouds are generated by taking different mesh element sizes (Table 4.5):

Table 4.5: # of Nodes generated with different mesh element sizes

hmax (mm)	**Node #**
15	131
13	259
12	497

As a result of the mesh sensitivity analysis for ϕ_m^N and ϕ_e^N and the study coming from Chapter 3 point cloud analysis, while constructing T maximum mesh element size must be selected as at least equal or smaller than element size of the converged mesh. Since Mesh 3 is the lower limit in which ϕ_m^N and ϕ_e^N are mesh independent anymore, it can be selected for T construction. However, here the important thing is that Mesh

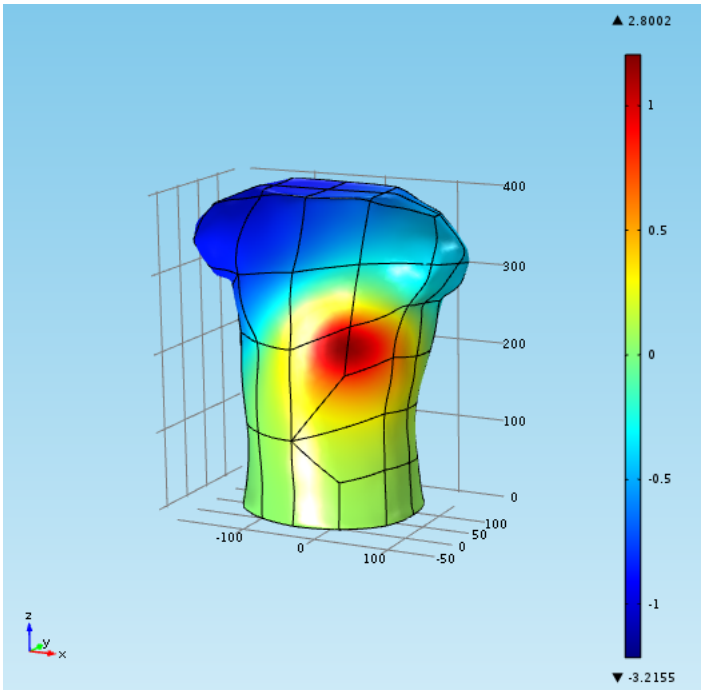

Figure 4.4: Torso ϕ_e^N potential distribution during epicardial ventricular depolarization. Color bar in (mV).

3 can not be applied on the geometry where nodes of the point clouds are defined. For this region, mesh must be selected in a manner so that it will divide the distance between the nodes to at least five. Therefore, by considering mesh element sizes given on Table 4.5, if hmax is selected as $12(mm)$ to create point cloud, mesh size for T construction must be selected at least $2.4(mm)$.

As explained in Chapter 3, column numbers of T are identified by the number of nodes in the point cloud and row numbers of T are identified by the fixed potential measurement locations. In this study, T is constructed from 9 fixed measurement locations critical for ECG signal interpretation on the surface of torso (see Figure 4.2) for three point cloud combinations given by Table 4.5. Then by using Equation 3.7, $[\phi_e^P]$ values are obtained by multiplying the constructed T for each point cloud with converged $[\phi_m^N]$ values calculated at corresponding node coordinates. The following equations gives $[\phi_e^P]$ values for each point cloud :

$$[T]_{9\times131}[\phi_m^N]_{131\times1} = [\phi_e^P]_{9\times1} \tag{4.1}$$

$$[T]_{9\times259}[\phi_m^N]_{259\times1} = [\phi_e^P]_{9\times1} \tag{4.2}$$

$$[T]_{9\times497}[\phi_m^N]_{497\times1} = [\phi_e^P]_{9\times1} \tag{4.3}$$

As in the case explained in Chapter 3, point cloud modeling results approach to converged solution by increasing number of nodes in the point clouds. Table 4.6 gives $[\phi_e^P]_{9\times1}$ value obtained by using 497 nodes with converged solution $[\phi_e^D]_{9\times1}$ and Figure 4.5 shows plots of the potential values at this table.

Table 4.6: Comparison of $[\phi_e^P]_{9\times1}$ value of 497 nodes with converged solution $[\phi_e^D]_{9\times1}$

Measurement Locations	$[\phi_e^D]_{9\times1}$ **(mV)**	$[\phi_e^P]_{9\times1}$ **(mV)**
RA	-1.06	-1.07
LA	-0.12	-0.11
LL	0.89	0.91
V1	0.49	0.51
V2	1.75	1.79
V3	2.63	2.67
V4	2.96	3.00
V5	2.64	2.68
V6	1.90	1.94

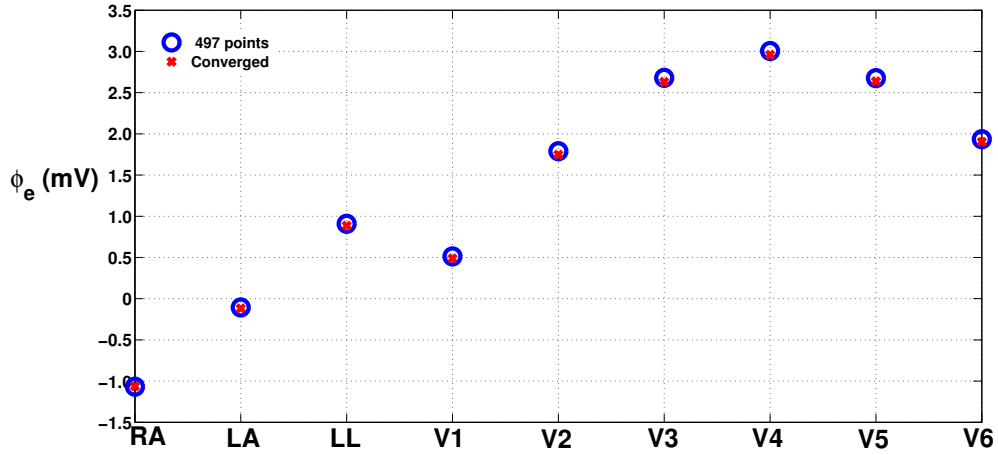

Figure 4.5: Plots of $[\phi_e^P]_{9\times1}$ value of 497 nodes with converged solution $[\phi_e^D]_{9\times1}$

CHAPTER 5

CONCLUDING REMARKS

In this study, bidomain model based transmembrane potential (TMP) distribution was used as equivalent cardiac source in order to examine the cellular electrophysiology macroscopically. Equivalent TMP distribution was generated by using a centric current dipole source and does not reflect the realistic TMP distribution within the heart. The main purpose of this study was to construct forward transfer matrix T and verify its accuracy by analytical solution. Therefore, in the first part of the study, both heart and torso were assumed as two concentric spheres and electrically isotropic regions. First, the forward problem of ECG was solved analytically. Then, TMP based transfer matrix, T was constructed by using point cloud modeling and the accuracy of T was verified by analytical solutions. In the second part of the study, a sphere representing heart was placed inside of a realistic torso to show the applicability of the point cloud modeling to any irregular geometry. By this purpose, the forward problem was solved and T is constructed again.

Although the idea of point cloud modeling comes from another study, this thesis made contribution to the literature by verifying the results of the point cloud modeling with analytical solution. Although COMSOL is used for finite element mesh generation, MATLAB code for point cloud modeling is written to construct T by using MATLAB Livelink of COMSOL. Then, numerical solution with point cloud modeling was analyzed according to both mesh sensitivity and intensity of the nodes in the point cloud. As a result of this study, it is suggested to take the distance between the nodes as uniform for point cloud generation. Here, the thing to be careful is to select the mesh element size of the geometry where points are located as if it will divide the distance

between the nodes to at least five mesh elements. Also, it is important to note that selected mesh element size for both geometries that represent heart and torso must be chosen as at least equal or smaller than the mesh element size of converged solution. Since the number of nodes and mesh element size are the main factors affecting the computational costs, for the studies where results show convergence at very small mesh element sizes with high number of nodes, it may be really difficult to obtain T with today's computer technology.

Another important inference of this study is that as long as there is no change at electrical conductivity and geometry of a volume conductor, there is no need to construct transfer matrix again and again. Because, the forward transfer matrix carries only static information about volume conductor of each patient. Therefore, if the volume conductor is same, it is unnecessary to construct a new transfer matrix for different TMP distributions within the heart.

As future work, the main purpose is to apply point cloud modeling to a generic heart model placed inside of a torso with more realistic equivalent TMP sources varying with time. By this way, the main objective is to observe the ECG signal accurately. Secondly, same study will be repeated by including fiber orientation of the cardiac muscle and thereby anisotropy into the solution domain. On the other hand, analytical solution can be derived again for different dipole and reference potential locations. By following the same steps in this study, new analytical solution can be compared with the results of point cloud modeling.

REFERENCES

[1] Leo K Cheng. *Non-invasive electrical imaging of the heart*. PhD thesis, ResearchSpace@ Auckland, 2001.

[2] www.who.int [Last accessed on 2015-02-26].

[3] Jaakko Malmivuo and Robert Plonsey. *Bioelectromagnetism: principles and applications of bioelectric and biomagnetic fields*. Oxford University Press, 1995.

[4] Bernd Messnarz, Bernhard Tilg, Robert Modre, Gerald Fischer, and Friedrich Hanser. A new spatiotemporal regularization approach for reconstruction of cardiac transmembrane potential patterns. *Biomedical Engineering, IEEE Transactions on*, 51(2):273–281, 2004.

[5] Dmytro Farina. *Forward and Inverse Problems of Electrocardiography: Clinical Investigations*. PhD thesis, Karlsruhe, 2008.

[6] Paul A Iaizzo. *Handbook of cardiac anatomy, physiology, and devices*. Springer, 2009.

[7] Henry Gray and Charles Mayo Goss. Anatomy of the human body. *American Journal of Physical Medicine & Rehabilitation*, 53(6):293, 1974.

[8] http://www.gwheartandvascular.org/education/anatomy-and-function-of-the-heart-valves/ [Last accessed on 2015-02-26].

[9] http://faculty.stcc.edu/aandp/ap/ap2pages/units18to20/heart/heart.htm [Last accessed on 2015-02-26].

[10] Joakim Sundnes, Glenn Terje Lines, Xing Cai, Bjørn Frederik Nielsen, Kent-Andre Mardal, and Aslak Tveito. *Computing the electrical activity in the heart*, volume 1. Springer, 2007.

[11] http://www.hkma.org/english/cme/onlinecme/cme201006main.htm [Last accessed on 2015-02-26].

[12] GT Lines, ML Buist, P Grottum, AJ Pullan, J Sundnes, and A Tveito. Mathematical models and numerical methods for the forward problem in cardiac electrophysiology. *Computing and Visualization in Science*, 5(4):215–239, 2003.

[13] Mike Lewell and Matthew Davis. 12 lead ecg. 2011.

[14] http://ifastfacts.com/ifastfacts-contents/ecg-2/12-lead-ecg-to-localize-myocardial-ischemia-injury-infarct.vmez2ryfnfo [Last accessed on 2015-02-26].

[15] http://www.ems12lead.com/2012/06/13/56-year-old-female-cc-short-of-breath-conclusion/ [Last accessed on 2015-02-26].

[16] Laura Bear, Phillip S Cuculich, Olivier Bernus, Igor Efimov, and Rémi Dubois. Introduction to noninvasive cardiac mapping. *Cardiac Electrophysiology Clinics*, 7(1):1–16, 2015.

[17] GF Shou, L Xia, HL Duan, and MQ Qian. Towards the cardiac equivalent source models in electrocardiography and magnetocardiography: A simulation study. In *Computing in Cardiology, 2010*, pages 859–862. IEEE, 2010.

[18] Robert S MacLeod and Dana H Brooks. Recent progress in inverse problems in electrocardiology. *Engineering in Medicine and Biology Magazine, IEEE*, 17(1):73–83, 1998.

[19] Guofa Shou, Ling Xia, Mingfeng Jiang, Qing Wei, Feng Liu, and Stuart Crozier. Truncated total least squares: a new regularization method for the solution of ecg inverse problems. *Biomedical Engineering, IEEE Transactions on*, 55(4):1327–1335, 2008.

[20] Ramesh M Gulrajani. The forward problem of electrocardiography: Theoretical underpinnings and applications. In *Modeling and Imaging of Bioelectrical Activity*, pages 43–79. Springer, 2005.

[21] Mark Potse, Bruno Dubé, and Alain Vinet. Cardiac anisotropy in boundary-element models for the electrocardiogram. *Medical & biological engineering & computing*, 47(7):719–729, 2009.

[22] G Fischer, B Tilg, P Wach, R Modre, U Leder, and H Nowak. Application of high-order boundary elements to the electrocardiographic inverse problem. *Computer methods and programs in biomedicine*, 58(2):119–131, 1999.

[23] A Steward Ferguson and Gerhard Stroink. Factors affecting the accuracy of the boundary element method in the forward problem. i. calculating surface potentials. *Biomedical Engineering, IEEE Transactions on*, 44(11):1139–1155, 1997.

[24] Christopher R Johnson. Computational and numerical methods for bioelectric field problems. *Critical Reviews? in Biomedical Engineering*, 25(1), 1997.

[25] Gaddam Chandra Mohan and Swapna Devi. Forward problem in electrocardiogram: A review of certain approaches. *IOSR Journal of Engineering*, 3:21–24, 2013.

[26] Pasi Kauppinen, Jari Hyttinen, Päivi Laarne, and Jaakko Malmivuo. A software implementation for detailed volume conductor modelling in electrophysiology using finite difference method. *Computer methods and programs in biomedicine*, 58(2):191–203, 1999.

[27] ZS Li, SA Zhu, and Bin He. Solving the ecg forward problem by means of a meshless finite element method. *Physics in medicine and biology*, 52(13):N287, 2007.

[28] Zhongshi Li, Yingchun Zhang, Shanan Zhu, and Bin He. Comparison of meshless fem and conventional fem for solving ecg forward problem: A simulation study. pages 274–275, 2007.

[29] Ramesh M Gulrajani. The forward problem of electrocardiography: from heart models to body surface potentials. In *Engineering in Medicine and Biology Society, 1997. Proceedings of the 19th Annual International Conference of the IEEE*, volume 6, pages 2604–2609. IEEE, 1997.

[30] Masanori Aoki, Yoshiwo Okamoto, Toshimitsu Musha, and Ken-Ichi Harumi. Three-dimensional simulation of the ventricular depolarization and repolarization processes and body surface potentials: Nornal heart and bundle branch block. *Biomedical Engineering, IEEE Transactions on*, 52(6):454–462, 1987.

[31] Ramesh M Gulrajani and Guy E Mailloux. A simulation study of the effects of torso inhomogeneities on electrocardiographic potentials, using realistic heart and torso models. *Circulation Research*, 52(1):45–56, 1983.

[32] Darrell J Swenson, Sarah E Geneser, Jeroen G Stinstra, Robert M Kirby, and Rob S MacLeod. Cardiac position sensitivity study in the electrocardiographic forward problem using stochastic collocation and boundary element methods. *Annals of biomedical engineering*, 39(12):2900–2910, 2011.

[33] Allan Van Oosterom and TF Oostendorp. Ecgsim: an interactive tool for studying the genesis of qrst waveforms. *Heart*, 90(2):165–168, 2004.

[34] Michael Seger, Gerald Fischer, Robert Modre, Bernd Messnarz, Friedrich Hanser, and Bernhard Tilg. Lead field computation for the electrocardiographic inverse problem, finite elements versus boundary elements. *Computer methods and programs in biomedicine*, 77(3):241–252, 2005.

[35] Adriaan Van Oosterom. Genesis of the t wave as based on an equivalent surface source model. *J. Electrocardiology*, 34(4):217–227, 2001.

[36] Adriaan van Oosterom and Vincent Jacquemet. Genesis of the p wave: atrial signals as generated by the equivalent double layer source model. *Europace*, 7(s2):S21–S29, 2005.

[37] Daming Wei, Osamu Okazaki, Kenichi Harumi, Eishi Harasawa, and H Hosaka. Comparative simulation of excitation and body surface electrocardiogram with isotropic and anisotropic computer heart models. *Biomedical Engineering, IEEE Transactions on*, 42(4):343–357, 1995.

[38] HG Puurtinen, J Hyttinen, P Kauppinen, N Takano, P Laarne, and J Malmivuo. Application of lead field theory and computerized thorax modeling for the ecg inverse problem. In *Engineering in Medicine and Biology Society, 2001. Proceedings of the 23rd Annual International Conference of the IEEE*, volume 1, pages 363–366. IEEE, 2001.

[39] Yves Coudière, Charles Pierre, RODOPLPHE Turpault, et al. Solving the fully coupled heart and torso problems of electro cardiology with a 3d discrete duality finite volume method. *submitted for publication*, 2006.

[40] Yasuo Yamashita and Takashi Takahashi. Use of the finite element method to determine epicardial from body surface potentials under a realistic torso model. *Biomedical Engineering, IEEE Transactions on*, (9):611–621, 1984.

[41] Yasuo Yamashita. Inverse solution in electrocardiography: determining epicardial from body surface maps by using the finite element method. *Japanese circulation journal*, 45(11):1312–1322, 1981.

[42] Yongmin Kim. A three-dimensional modifiable computer body model and its applications. 1982.

[43] A Vahid Shahidi, Pierre Savard, and Réginald Nadeau. Forward and inverse problems of electrocardiography: modeling and recovery of epicardial potentials in humans. *Biomedical Engineering, IEEE Transactions on*, 41(3):249–256, 1994.

[44] Christopher R Johnson, Robert S MacLeod, and Philip R Ershler. A computer model for the study of electrical current flow in the human thorax. *Computers in Biology and Medicine*, 22(5):305–323, 1992.

[45] A Pullan. A high-order coupled finite element/boundary element torso model. *Biomedical Engineering, IEEE Transactions on*, 43(3):292–298, 1996.

[46] A Vahld Shahidi and P Savard. Forward problem of electrocardiography: construction of human torso models and field calculations using finite element method. *Medical and Biological Engineering and Computing*, 32(1):S25–S33, 1994.

[47] Shankarjee Krishnamoorthi, Luigi E Perotti, Nils P Borgstrom, Olujimi A Ajijola, Anna Frid, Aditya V Ponnaluri, James N Weiss, Zhilin Qu, William S Klug, Daniel B Ennis, et al. Simulation methods and validation criteria for modeling cardiac ventricular electrophysiology. *PloS one*, 9(12):e114494, 2014.

[48] I Aitidis, E Gogou, P Bonovas, H Panagiotidis, and G Kyriacou. Equivalent cardiac dipole localization from ecg data using proper orthogonal decomposition. In *Biomedical Engineering, 2011 10th International Workshop on*, pages 1–4. IEEE, 2011.

[49] JUN-ICHI OKADA, Teruyoshi Sasaki, Takumi Washio, Hiroshi Yamashita, Taro Kariya, Yasushi Imai, Machiko Nakagawa, Yoshimasa Kadooka, Ryozo Nagai, Toshiaki Hisada, et al. Patient specific simulation of body surface ecg using the finite element method. *Pacing and Clinical Electrophysiology*, 36(3):309–321, 2013.

[50] Dafang Wang, Robert M Kirby, and Chris R Johnson. Finite element discretization strategies for the inverse electrocardiographic (ecg) problem. In *World Congress on Medical Physics and Biomedical Engineering, September 7-12, 2009, Munich, Germany*, pages 729–732. Springer, 2009.

[51] Robert Modre, Michael Seger, Gerald Fischer, C Hintermuller, Dieter Hayn, Bernhard Pfeifer, Friedrich Hanser, Günter Schreier, and Bernhard Tilg. Cardiac anisotropy: is it negligible regarding noninvasive activation time imaging? *Biomedical Engineering, IEEE Transactions on*, 53(4):569–580, 2006.

[52] THEO C Pilkington, Mary N Morrow, and PEGGY C Stanley. A comparison of finite element and integral equation formulations for the calculation of electrocardiographic potentials. *Biomedical Engineering, IEEE Transactions on*, (2):166–173, 1985.

[53] Martin Buist and Andrew Pullan. Torso coupling techniques for the forward problem of electrocardiography. *Annals of biomedical engineering*, 30(10):1299–1312, 2002.

[54] Bin He, Guanglin Li, and Xin Zhang. Noninvasive imaging of cardiac transmembrane potentials within three-dimensional myocardium by means of a realistic geometry anisotropic heart model. *Biomedical Engineering, IEEE Transactions on*, 50(10):1190–1202, 2003.

[55] D Farina, Y Jiang, O Skipa, O Dossel, C Kaltwasser, and WR Bauer. The use of the simulation results as a priori information to solve the inverse problem of electrocardiography for a patient. In *Computers in Cardiology, 2005*, pages 571–574. IEEE, 2005.

[56] Linwei Wang, Ken CL Wong, Heye Zhang, and Pengcheng Shi. Electrocardiographic simulation on coupled meshfree-bem platform. In *Functional Imaging and Modeling of the Heart*, pages 162–171. Springer, 2009.

[57] Marie Dupraz, Simonetta Filippi, Alessio Gizzi, Alfio Quarteroni, and Ricardo Ruiz-Baier. Finite element and finite volume-element simulation of pseudo-ecgs and cardiac alternans. *Mathematical Methods in the Applied Sciences*, 2014.

[58] WHW Schulze, B Wang, D Potyagaylo, and O Dössel. Use of a tolerance operator in wavefront-based ecg imaging of transmembrane voltages. In *World Congress on Medical Physics and Biomedical Engineering May 26-31, 2012, Beijing, China*, pages 422–425. Springer, 2013.

[59] Danila Potyagaylo, Max Segel, Walther HW Schulze, and Olaf Dössel. Non-invasive localization of ectopic foci: a new optimization approach for simultaneous reconstruction of transmembrane voltages and epicardial potentials. In *Functional Imaging and Modeling of the Heart*, pages 166–173. Springer, 2013.

[60] Mingfeng Jiang, Yaming Wang, Ling Xia, Feng Liu, Shanshan Jiang, and Wenqing Huang. The combination of self-organizing feature maps and support vector regression for solving the inverse ecg problem. *Computers & Mathematics with Applications*, 66(10):1981–1990, 2013.

[61] Matthew NO Sadiku. *Numerical techniques in electromagnetics*. CRC press, 2000.